www.sciencemag.org/cgi/content/full/science.aaj2155/DC1

Supplementary Materials for

mTOR regulates metabolic adaptation of APCs in the lung and controls the outcome of allergic inflammation

Charles Sinclair,* Gayathri Bommakanti,* Luiz Gardinassi, Jens Loebbermann, Matthew Joseph Johnson, Paul Hakimpour, Thomas Hagan, Lydia Benitez, Andrei Todor, Deepa Machiah, Timothy Oriss, Anuradha Ray, Steven Bosinger, Rajesh Ravindran, Shuzhao Li, Bali Pulendran†

*These authors contributed equally to this work.
†Corresponding author. Email: bpulend@emory.edu; bpulend@stanford.edu

Published 10 August 2017 on *Science* First Release
DOI: 10.1126/science.aaj2155

This PDF file includes:

Materials and Methods

Mice

Mice were bred and housed at Yerkes National Primate Research Center vivarium (Emory University, Atlanta, GA), under specific pathogen-free conditions. Experimental mice were used between 5-12 weeks of age. All animal protocols were reviewed and approved by the Emory University Institutional Animal Care and Use Committee (IACUC). Mouse genotyping was confirmed using standard PCR analysis of ear biopsies. Mouse strains originated from The Jackson Laboratory (JAX) and were on a C57BL/6J background or bred in-house unless indicated.

The following strains of mice were used in this study: C57BL/6J (CD45.2+), B6.SJL-*Ptprc*^{a} *Pepc*^{b}*/BoyJ* (CD45.1^{+}) or (C57BL/6J x B6.SJL-*Ptprc*^{a} *Pepc*^{b}*/BoyJ*)F1 (B6 CD45.1^{+}/CD45.2^{+}) were used as WT strains. CD11c-Cre$^{+/-}$ *mTOR*$^{fl/fl}$ mice (mTOR$^{\Delta APC}$) were generated by breeding B6.129S4-Mtor$^{tm1.2Koz/J}$ (*mTOR*$^{fl/fl}$) mice (*44*) with B6.Cg-Tg(Itgax-cre)1-1Reiz/J (CD11c-Cre) (*45*), controls were CD11c-Cre- littermates or C57BL/6J. CD11c-Cre$^{+/-}$ *Raptor*$^{fl/fl}$ mice (Raptor$^{\Delta APC}$) were generated by crossing B6.Cg-Rptor$^{tm1.1Dmsa/J}$ (*Raptor*$^{fl/fl}$) mice with CD11c-Cre (*46*), controls were CD11c-Cre- littermates or C57BL/6J. CD11c-Cre$^{+/-}$ *Rictor*$^{fl/fl}$ mice (Rictor$^{\Delta APC}$) were generated by crossing Rictor$^{tm1.1Klg/SjmJ}$ (*Rictor*$^{fl/fl}$) mice with CD11c-Cre (*47*), controls were CD11c-Cre^{-} littermates.129S-Batf3$^{tm1Kmm/J}$ (*Batf3*$^{-/-}$) mice (*48*) were purchased directly from JAX, and compared to C57BL/6J controls. *S6k1*$^{-/-}$*S6k2*$^{-/-}$ mice (S6K1/2 dKO) were kindly provided by professor Sara C. Kozma (University of Cincinnati, Cincinnati, USA) and Nahum Sonenberg (McGill University, Montreal, Canada) have been described previously (*49*), and were on a mixed C57BL/6-129/Ola background. This strain was maintained by intercrossing *S6k1*$^{+/-}$*S6k2*$^{+/-}$ breeders. *S6k1*$^{+/+}$*S6k2*$^{+/+}$ littermates were used as control. *4ebp1*$^{-/-}$*4ebp2*$^{-/-}$ (4EBP1/2 dKO) mice (*50*) were a kind gift from Prof. Nahum Sonenberg (McGill University, Montreal, Canada), and were backcrossed onto a C57BL/6J background in-house for ≥ 10 generations. C57BL/6J were used as control. mTOR$^{\Delta APC}$ 4EBP1/2 dKO mice were generated by crossing mTOR$^{\Delta APC}$ and *4ebp1*$^{-/-}$*4ebp2*$^{-/-}$ strains. CD11c-Cre$^{+/-}$ *Hif1a*$^{fl/fl}$ (Hif1α$^{\Delta APC}$) were generated by crossing B6.129-Hif1a$^{tm3Rsjo/J}$
(Jackson Labs) with CD11c-Cre (*51)*. Controls were CD11c-Cre- littermates or C57BL/6J.

In vivo administration of substances to mice

BrdU (BD Pharmingen, 2mg/mouse) was administered q.d. for 2d according to manufacturer's instructions. The Srebp1/2 inhibitor Fatostatin (*52*) was formulated in 10% DMSO and 30mg/kg was administered q.d. in 150µL injection volume i.p. for 10d. Rapamycin (Selleck Chemicals) was formulated in 49.5% PBS, 49.5% PEG400 (Sigma) and 1% DMSO vehicle, and administered q.d. (1.8mg/kg loading dose, 0.6mg/kg maintenance dose) in 100µL injection volume i.p. for 10d. Clodronate or control liposomes (Clodrosome) were administered by i.t. installation of 50µL suspension to anaesthetized mice. Etomoxir was dosed i.p. in 150µL PBS 3x weekly.

Media

Unless indicated, incomplete Hank's Balanced Salt Solution (HBSS) additionally contained 2% FCS (Corning) and 10mM HEPES (Lonza/Gibco). BAL media was PBS containing 5mM EDTA. FACS buffer refers to PBS containing 0.5% Bovine Serum

Albumin (BSA, Sigma). MACS buffer was PBS containing 0.2% BSA and 2mM EDTA (Corning). Complete RPMI (cRPMI) contained 10% FCS (Gemini Benchmark), 10mM HEPES, 2mM Glutamine, 1X non-essential amino acids, 1mM sodium pyruvate, 1X antibiotic/antimycotic (all purchased from Gibco or Lonza). ELISA blocking buffer was PBS containing 1% BSA (w/v)/0.5% Tween20 (v/v)).

Preparation of single cell suspensions

Spleens were finely chopped with a scalpel in 6-well plates, and digested with 1-1.5mg/mL collagenase type 4 (Worthington Biochemical Corporation) dissolved in HBSS. Digestion was performed for 30 minutes at 37°C, and reactions were stopped with addition of 2mM EDTA. Digestions were passed through 40µm cell strainers to obtain a homogenous cell suspension.

Kidney was prepared similarly to spleen and thymi, with the exception that collagenase digestion was performed for 45 minutes.

Skin draining (superficial cervical, axillary, brachial and inguinal), mediastinal and mesenteric lymph nodes were gently burst with a 3mL syringe plunger thumb rest, and digested with 1-1.5mg/mL collagenase type 4 for 20-25 minutes at 37°C. Reactions were stopped with 2mM EDTA and digestions passed through 40µm cell strainers.

To obtain lung suspensions, mice were sacrificed with CO2 and perfused with 5mL PBS injected into the right ventricle. Lungs were dissected into gentleMACS™ C tubes (Miltenyi) and dissociated using a gentleMACS™ octo dissociator using the pre-set program m_lung_01_02. Dissociated lung was digested with 1-1.5mg/mL collagenase type 4 for 30 minutes at 37°C. Lungs were next homogenized with gentleMACS™ octo dissociator program m_lung_02_01, reactions were stopped with 2mM EDTA and digestions passed through 40µm cell strainers. Cells were pelleted (1500-2000rpm/300-500xg for 5 minutes). Red blood cells were lysed with 1mL Ack lysing buffer (Lonza) for 1 minute and lysis was stopped by addition of ≥ 5 volumes of HBSS. Cells were washed once to obtain single cell suspensions.

To obtain Bronchoalveolar Lavage (BAL) cells, mice were sacrificed with CO2, tracheas were exposed, and mice were pinned upright to a dissection board. Tracheas were incised laterally with a scalpel blade. BAL fluid was obtained by inserting a blunted 22G needle mounted with PE-50 tubing (BD) attached to a 3mL Luer lock syringe into the tracheal opening, and lavaging 3x with 1mL BAL media. BAL fluid was transferred to a 1.5mL eppendorph tube, and cells were pelleted in a microcentrifuge for 5 minutes (3000RPM/500xg). Red blood cells were lysed with 200µL Ack lysing buffer for 1 minute, and lysis was stopped by addition of 4 volumes of HBSS. Leukocytes were washed once to obtain single cell suspensions.

To prepare dermal and epidermal suspensions, ears were dissected, split into dorsal and ventral halves, and floated dermal side down on solution containing 1.25mg/mL purified Neutral Protease (Dispase) (Worthington Biochemical Corporation) dissolved in HBSS (FCS-free) for 45-60 minutes at 37°C. Ear halves were then placed epidermal side down on polystyrene tissue culture plate lids, and dermal layers were gently peeled from the epidermis using micro-dissecting forceps. Dermal and epidermal fractions were finely chopped in 6-well plates containing 1-1.5mg/mL collagenase type 4 for 1 hour at 37°C. Reactions were stopped with 2mM EDTA and digestions passed through 40µm cell strainers to obtain single cell suspensions.

Liver was coarsely chopped with dissection scissors, and digested with collagenase IV for 30' at 37°C. The reaction was stopped with addition of 2mM EDTA, digestions were sequentially passed through 70µm and 40µm cell strainers, and hepatocytes were removed via differential centrifugation (300RPM/10xg) for 5 minutes. Leukocyte-containing supernatant transferred to a fresh tube and washed 1x, stained CD11c and CD11b microbeads (Miltenyi) and further enriched for APCs using MACS manual separation (Miltenyi), according to manufacturer's protocols. Alternatively for T-cell assays, mononuclear populations were enriched from leukocyte-containing supernatant after centrifugation (1500RPM, 15'), at the interphase of a 70%/40% Percoll gradient.

Perigonadal white adipose tissue (WAT) was finely diced with dissection scissors in 6-well plates, and digested with collagenase IV for 45' at 37°C. Digestions were gently agitated via gentle stirring every 10 minutes. Cells were passed sequentially through 70µm and 40µm cell strainers. The stromal vascular fraction (SVF) was isolated from adipocytes via differential centrifugation (1300RPM/200xg) for 10 minutes. Supernatant was removed by aspiration and cell pellets were washed 2x with HBSS.

Large intestine was cut longitudinally and luminal contents were removed with forceps and via sequential washes in an HBSS bath. Intestinal tissue was sectioned into 1.5cm fragments, and epithelia was removed by incubating with HBSS (additionally containing 1mM DTT and 5mM EDTA), in a shaking incubator at 37°C for 20 minutes. Samples were then washed 1x with HBSS (FCS-free) for 10 minutes at 37°C. Lamina propria fragments were transferred to a gentleMACS™ C tubes and digested with 0.6g/mL Collagenase type VIII (Sigma) in HBSS for 30 minutes at 37°C in a shaking incubator. Samples were homogenized with a gentleMACS™ octo dissociator using the pre-set program m_intestine_01, passed sequentially through 70µm and 40µm cell strainers, and washed 1x to obtain homogenous single cell suspensions.

To obtain bone marrow, epiphyses were removed from dissected tibiae and femora, and BM was obtained by flushing the medullary canal with HBSS. BM was then passed through a 40µm cell strainer.

Quantification of cell numbers

Cell counts were performed using a hemocytometer or with flow cytometric counting beads (BD Countbright absolute counting beads or Thermo Scientific Cyto-Cal™ count control beads), according to manufacturer's protocols.

Flow cytometry

Flow cytometric antibodies used in this study were purchased from Biolegend or eBioscience unless indicated and are listed in Table S1. Samples containing 2-5x10^6 cells were first stained using the Live/dead Fixable Aqua Staining Kit (Invitrogen) in 100µL PBS, for 15 minutes at 4°C in the dark. Cells were washed 1x with FACS buffer, and detection of surface antigens was performed by incubation with antibody cocktails in 100µL FACS buffer for 25 minutes at 4°C in the dark. For detection total mTOR, cells were fixed with Cytofix/Cytoperm solution (BD) for 15 minutes, washed twice, and incubated with intracellular antibody for 60 minutes.

To detect CXCR5, samples were first incubated with primary rat anti-mouse CXCR5 for two hours, followed by secondary goat anti-rat conjugated to Biotin for one hour, in FACS buffer. Cells were next stained with Live/dead Aqua in PBS for 15

minutes at 4°C, washed, and incubated with antibody cocktail containing streptavidin conjugated to Brilliant Violet 421™ and other surface antigens in FACS buffer, for 30 minutes at 4°C.

Intracellular detection of BrdU was performed using an APC BrdU flow kit (BD Pharmingen), according to manufacturer's instruction.

For intracellular detection of cytokines, cells were stained with Live/Dead Aqua for 10' and immediately fixed for 15 minutes with Cytofix/Cytoperm solution. After two washes, surface antigens and cytokines were detected simultaneously by incubation with antibody cocktails in 100µL 1X Perm/Wash buffer (BD) for 25 minutes at 4°C.

Phospho-specific epitopes were detected by immediately fixing cells with Cytofix/Cytoperm solution, washing twice, and incubating with staining cocktails containing both surface and intracellular antibodies for 30 minutes at 4°C.

Samples we filtered through 40µm cell strainers before acquisition using BD LSRFortessa or BD LSRII flow cytometers and BD FACS DIVA software. Data compensation and downstream analysis was performed using FlowJo software v9.8.5 (Tree Star).

Cell sorting

DCs were enriched with CD11c and CD11b microbeads and MACS manual separation (Miltenyi), according to the manufacturer's instructions. Enriched cells were stained with live/dead Aqua or Via-Probe™ (BD) and with surface antibody cocktails. Populations were further purified to ≥95% purity with a BD FACSAria cell sorter.

PCR

Genomic DNA was prepared using the Quanta AccuStart II Mouse Genotyping Kit, as per the manufacturer's instructions, and PCR reactions were resolved on an agarose gel (1.5% w/v) containing 5µg/mL ethidium bromide. Excised mTOR was detected by the presence of a 700bp DNA fragment from PCR reactions containing the mTOR-out-F (TTATGTTTGATAATTGCAGTTTTGGCTAGCAGT) and mTOR-R (TTTAGGACTCCTTCTGTGACATACATTTCCT) primers. Non-deleted mTOR was detected by the presence of a 533bp DNA fragment from PCR reactions using the mTOR-in-F (GTTAGCCTCTAGACTCCCTCAGACC) and mTOR-R primers. Genomic CD11c-Cre was detected by the present of a 313bp product using the CD11c-Cre-F (ACTTGGCAGCTGTCTCCAAG) and CD11c-Cre-R (GCGAACATCTTCAGGTTCTG) primers.

Generation of murine bone marrow derived dendritic cells (BMDCs)

Bone marrow (BM) was cultured in complete RPMI supplemented with 20ng/mL murine GM-CSF (Peprotech), at a concentration of 1-2x10^6 cells/mL in 10mL volume, on 100x20mm petri dishes. Cell cultures were re-fed by complete replacement of media on day 3 and day 6.

BMDCs were harvested on d8. Loosely adherent cells were dissociated from petri dishes using a cell scraper. Both loosely adherent and non-adherent cells were passed through a 70µm cell strainer, stained with CD11c magnetic microbeads, and enriched to ≥95% purity by MACS manual separation, according to the manufacturer's instructions.

Cell culture

Splenic DCs were enriched to ≥95% purity with CD11c magnetic microbeads and manual MACS separation. Splenic DCs and BMDCs were cultured in 200µL complete RPMI in 96-well round bottom tissue culture plates at a concentration of 1-1.25x10^6 cells/mL. Cells were stimulated with LPS (200ng/mL unless indicated, CpG-B (200ng/mL), Zymosan (25µg/mL) or Curdlan (25µg/mL) (all purchased from Invivogen). In some experiments, 5mM ATP (Thermo scientific) was added for the final hour of culture to elicit IL-1β production.

Primary APC survival cultures were performed with FACS sorted populations in complete RPMI for 24h. Where indicated Torin1 (250nM) was added to cultures.

Bone marrow chimeras

BM chimeras were performed essentially as described (*53*). Briefly, donor BM (2-5x10^6 cells) was transferred (i.v.) to lethally irradiated (2 x 550 rad) B6 CD45.1+ or B6 CD45.1^+/CD45.2^+ hosts. Chimeric mice were rested in sterile caging for a minimum of 8 weeks to allow for reconstitution.

RNA-seq

RNA was isolated from FACS purified populations using Trizol® according to manufacturer's instructions. Total RNA was amplified using the Clontech RNA amplification kit before library preparation and sequencing using Illumina Truseq (Illumina) and the Illumina pipeline, on an Illumina HiSeq system. Reads were normalized using the DESeq2 package in R. Pathway overrepresentation of differentially expressed genes was performed with innateDB (*54*). Gene networks were generated with STRING (*55*), using a high confidence interaction score. For transcription factor target analysis, target genes were identified using the TRANSFAC database.

Metabolomics

The metabolomics analysis was performed essentially as described (*56*). Acetonitrile (2:1, v/v) was added to cell extracts and proteins were removed by centrifugation at 14,000g for 10 min at 4 °C. The supernatant was transferred into autosampler vials for LC-MS analysis. Mass spectral data were collected on a Thermo Q-Exactive HF mass spectrometer (Thermo Fisher, San Diego, CA) coupled with a HILIC column, using positive ESI. The full scan of mass-to-charge ratio (m/z) ranged from 85 to 1250, with mass resolution at 120,000. Three analytical replicates were run for each sample and apLCMS software (v6.0.3) was used to extract and quantify metabolite features. Data were log2 transformed, averaged among analytical replicates and normalized by the mean. Only features detected in more than half of samples (4921) were used in further analysis. Student's t-test or one-way ANOVA were used for comparisons between cell subsets. The mummichog software (v1.0.7) was used for pathway analysis and tentative metabolite annotation (mass accuracy under 10 ppm) (*56*). Tentative annotations for sterol lipids was performed by accurate m/z matching to LIPID MAPS database (*57*). Among the metabolites in this study, over 40 were matched to confirmed in-house library, including threonine, asparagine, aspartate, lysine, methionine, xanthine, hypoxanthine, histidine, arginine, citrulline, tyrosine, kynurenine, L-carnitine, linoleic acid and linolenic acid.

House dust mite induced allergy

Mice were anesthetized with Isoflurane, and allergen was administered intranasally (i.n.) with 25µL house dust mite extract (HDM) (1mg/mL protein content, Greer Labs). For chronic HDM experiments, injections were performed thrice weekly and mice were analyzed after 18d. For short-term experiments, mice were deeply anesthetized with Isofluorance, and 75µg HDM was administered intratracheally on d0 and d2, before analysis on d3. In some experiments, mice received 400µg neutralizing mAbs thrice weekly i.p., on day -1 and then concurrent with HDM administration. The following mAb clones were purchased from BioXcell: α-IL12/23p40 (Clone R1-5D), α-IL12p70 (Clone R2-9A), α-Csf1r (Clone AFS98), or 400µg rat IgG2a isotype control (Clone 2A3).

MOG35-55/CFA induced experimental autoimmune encephalomyelitis (EAE) induction

EAE was induced using a Hooke kit™ MOG35-55/CFA Emulsion PTX kit (Cat. EK-2110, Hooke laboratories). Clinical scoring of mice was performed according to the manufacturer's instructions. Briefly, mice were vaccinated MOG35-55/CFA (administered as an emulsion in 2x 100µL s.c. injections), followed by two boosts with pertussis toxin (400ng, administered in 100µL i.p.) administered after 2h and 24h. Disease progression was monitored daily for 30d.

ELISA

Lung homogenate was prepared by dissociating whole lungs with the gentleMACS™ octo dissociator program m_lung_02_01 in 1mL PBS. Suspensions were passed through a 40µm cell strainer and clarified by centrifugation. Supernatant was used for cytokine ELISA.

Cytokines from lung homogenate or cell culture supernatant were measured by two-site sandwich ELISA. IL-6, TNFα (ELISA set II), IL-12p40, IL-12p70, IL-10, IL-1β and GM-CSF were measured using OptEIA™ ELISA sets (BD). M-CSF, Flt3L and IL-23 was measured using a murine Duoset ELISA kit (R&D systems). ELISAs were performed according to manufacturer's instructions, in 96-well polystyrene MaxiSorp ELISA plates (NUNC). Plates were coated overnight with detection antibody in PBS, then blocked with ELISA blocking buffer. After washing, cell supernatant was diluted 1:2 (TNFα, IL-12p70, IL-10, IL-1β, IL-23) or 1:10 (IL-6, IL-12p40) in blocking buffer and incubated on blocked plates in 100µL volume. Plates were washed and finally incubated with biotinylated detection antibodies and streptavidin conjugated to HRP.

To obtain serum, blood was obtained by tail vein bleeding, allowed to clot at room temperature for ≥4 hours, and cleared in a microcentrifuge (13,000RPM) for 15 minutes. Sera were stored at -80°C. For serum ELISAs, plates were coated overnight with 20µg/mL HDM protein, or 4µg/mL α-IgE (BD, clone R35-72). Plates were next incubated with ELISA blocking buffer for 30 minutes, then with serum diluted in ELISA blocking buffer for 1.5 hours. Antibodies were detected using HRP-conjugated α-IgG1 or IgE (all polyclonal, Southern Biotechnology), diluted 1/5000 in ELISA blocking buffer for 1.5 hours.

ELISA plates were developed with 100µL tetramethylbenzidine (TMB) substrate (BD), and reactions were stopped with addition of 50µL 2N H_2SO_4. Absorbance values were read on a model 680 spectrophotometer (Bio-rad) at 450nm with correction at

595nm by subtraction. Unknown samples were quantified by interpolation to a standard curve, calculated using the one-site specific binding function (non-linear regression, Y = Bmax*X/(Kd + X)), in Graphpad Prism (v6.0d). Antigen-specific serum Igs were compared to total Ig captured standards and expressed as arbitrary units (A.U.) to allow for pooling of experiments.

Ex vivo restimulation of T-cells

Restimulations were performed by culturing $\leq 5x10^6$ cells in 200µL complete RPMI at a concentration of $\leq 2.5x10^7$/mL, in 96-well tissue culture plates.

Restimulation with PMA and ionomycin was performed by culturing cells in round-bottomed plates with 1µg/mL Ionomycin and 100ng/mL PMA in the presence of 1x BD Golgi Plug (Brefeldin A) and 1x BD Golgi Stop (monensin), for 4h at 37°C.

Peptide restimulation was performed by culturing cells in round-bottomed plates for 4-5h in the presence of 2µg/mL α-CD28, 1x Golgi Stop and 1x Golgi Plug, and peptide pools containing each peptide at a concentration of 2.5µg/mL. The Flumist influenza peptide pool contained conserved Mhc-I restricted NP366-374 (ASNENMETM) and Mhc-II restricted NP311-325 (QVYSLIRPNENPAHK) peptides.

Flumist vaccination

Mice were anesthetized with Isoflurane (Attane USP, Piramal Critical Care), and vaccinated intranasally (i.n.) with 25µL ($1/8^{th}$ human dose) 2014-2015 Flumist® Quadrivalent Vaccine (Lot CH2021, Medimmune).

Histology

Lungs were inflated with 10% neutral buffered formalin, then fixed in 10% neutral buffered formalin for 24h and paraffin embedded (FFPE). FFPE samples were sectioned at 4µm, and stained with hematoxylin and eosin. The paraffin-embedded sections were subjected to deparaffinization in xylene, rehydration in graded series of ethanol, and rinsing with distilled water.

For Periodic Acid-Schiff (PAS) staining, FFPE sections were oxidized with periodic acid solution (0.5% w/v) for 5 minutes, then stained with Schiff reagent (Fisher) for 20 minutes. Slides were counterstained with hematoxylin before mounting.

For Immunohistochemical analysis, slides were subjected to antigen retrieval using DIVA Decloaker (Biocare, Concord, CA), following manufacturer's instructions. Slides were stained with primary α-Surfactant D (SP-D) antibody (Clone 12G5, Abcam), and secondary HRP-conjugated mouse on mouse polymer (biocare Medica). Reactions were detected using the Warp Red chromogen kit (Biocare Medical). Nuclei were then counter stained using Gill's hematoxylin.

To perform differential-quick analysis, BAL cells were cytospun onto frosted microsope slides (Fisher). Slides were fixed with 100% methanol and stained with self-buffered differential Wright-Giemsa stain (Quick stain II, Camco), as per the manufacturer's instructions.

Histological sections were analyzed and imaged using an Olympus BX-43F microscope equipped with Olympus Microfire camera, using Picture frame software.

Statistics

Statistical differences between serum antibody concentrations were determined using a Mann-Whitney test. ANOVA was used for multiple comparisons. All other statistical differences were calculated using a student's t-test unless indicated. Significance was denoted as follows: * $p \leq 0.05$, ** $p \leq 0.01$, *** $p \leq 0.001$, **** $p \leq 0.0001$. All analysis was performed using Graphpad Prism (v6.0g).

Supplementary Figures.

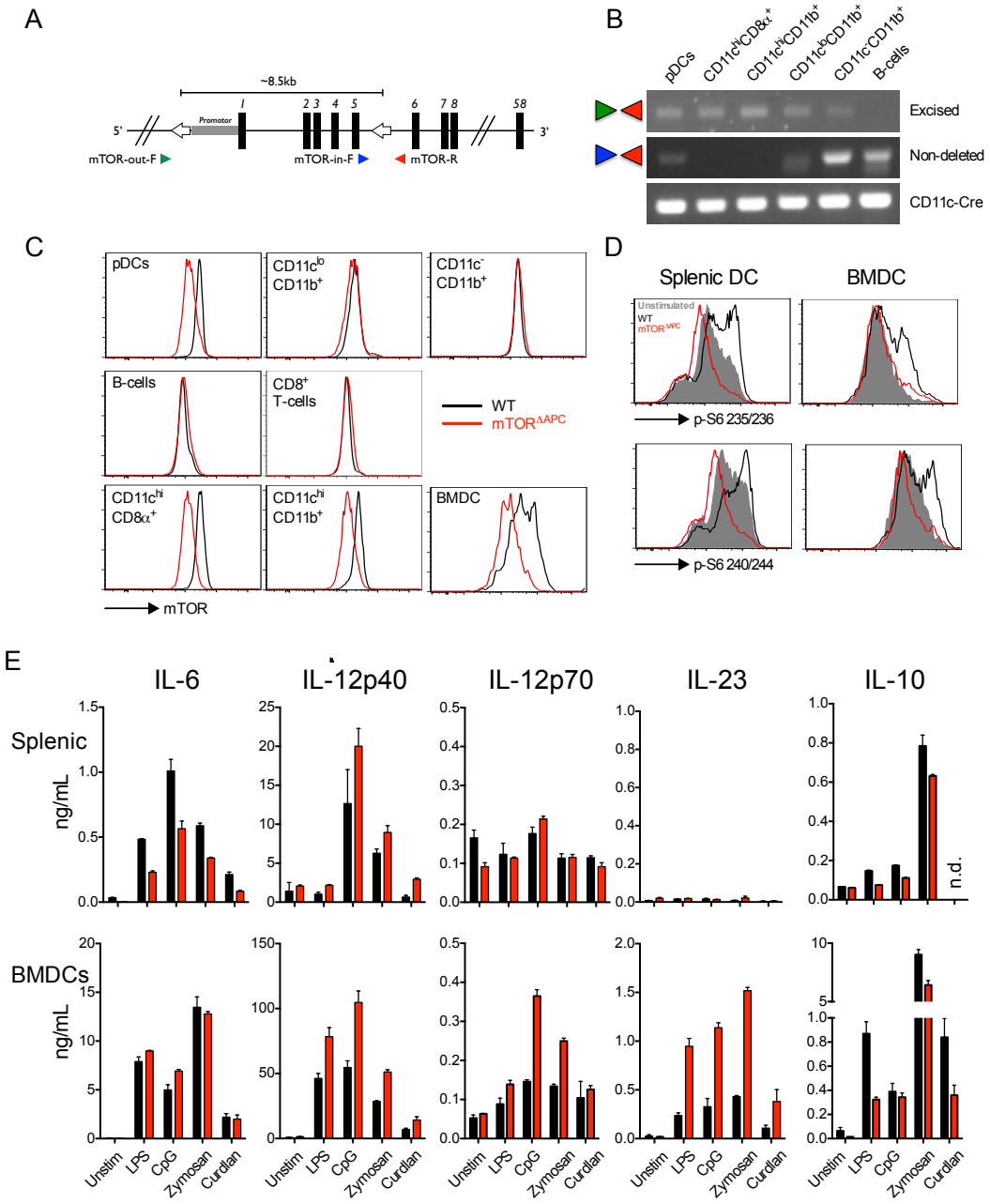

Fig. S1. Genetic ablation of the mTOR pathway recapitulates the phenotype of mTOR inhibited DCs.

CD11c-Cre$^{+/-}$ mice were interbred with mTOR$^{fl/fl}$ mice to genetically ablate mTOR in DCs. (**A**) Schematic diagram (not to scale) of the floxed mTOR locus, denoting exons (black rectangles), LoxP sites (white arrows) and genotyping primer locations (colored triangles). (**B**) PCR was performed on genomic DNA extracts from splenic populations. The top gel shows the presence of an excised (floxed-out) genomic mTOR^{fl} allele, the

middle gel shows the presence of a non-deleted allele, and the bottom control gel shows the presence of the CD11c-Cre transgene. Colored triangles denote primer pairs used in each reaction. (**C**) Histograms show total mTOR protein expression on indicated splenic and BMDC populations. (**D**) DCs were simulated with 1μg/mL LPS or left unstimulated for 24h, and analyzed by flow cytometry. Histograms show expression of phosphorylated S6 protein. (**E**) Splenic DCs or BMDCs were cultured for 24h with indicated ligands, and cytokines were measured by ELISA. Bar graphs show ELISA measurements of supernatant cytokine concentrations. Data represents ≥2 experiments (**A-D**) or ≥4 experiments.

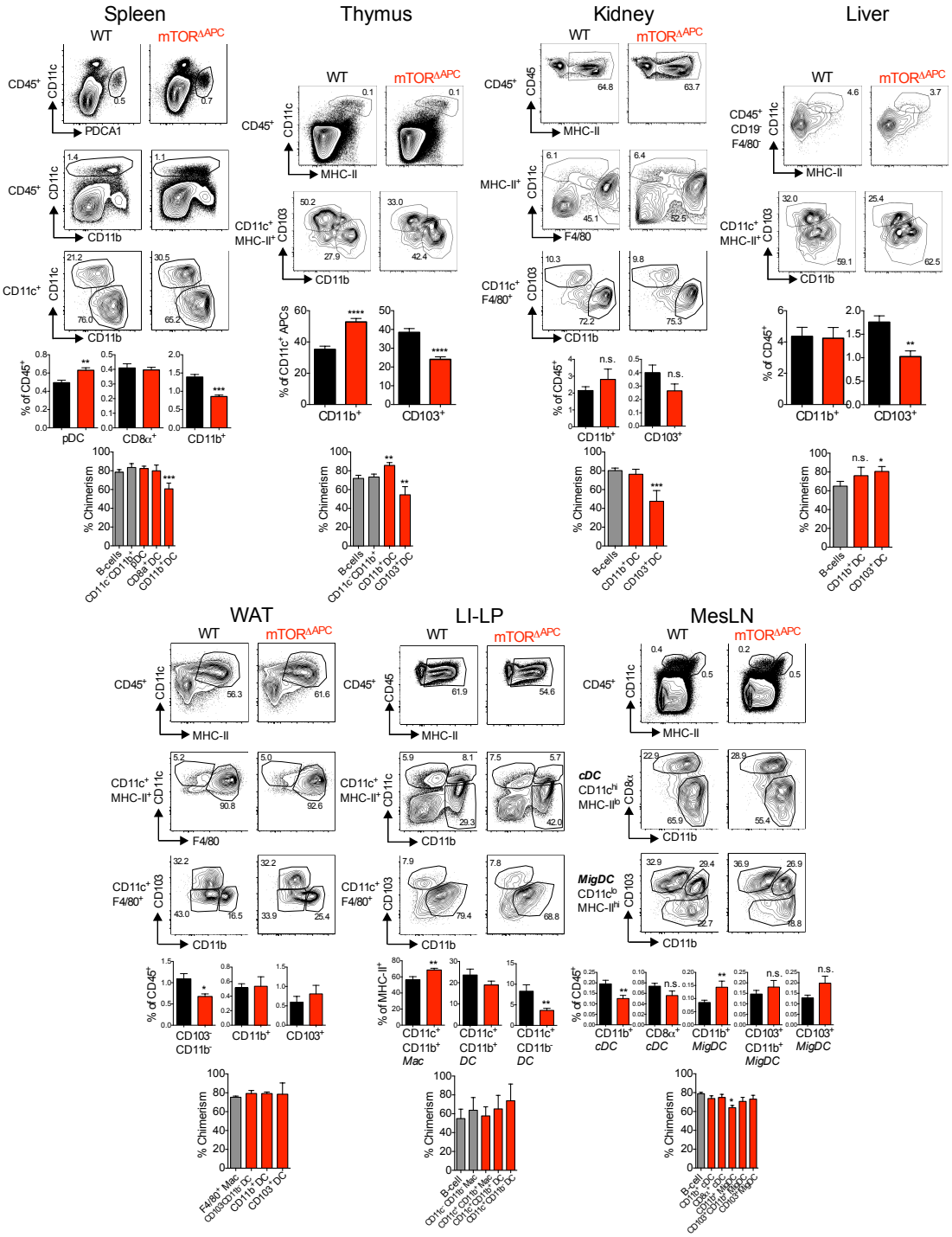

Fig. S2. Anatomically distinct roles for mTOR in DC homeostasis.

Contour plots show representative phenotypes and bar charts show pooled frequencies of indicated DC populations for WT (black) and mTOR$^{\Delta APC}$ (red). In addition, mixed bone marrow chimeras were established by mixing mTOR$^{\Delta APC}$ (CD45.2)

and B6 CD45.1 BM cells (3:1 ratio), and transferring them to B6 CD45.1^{+}/CD45.2^{+} hosts. Lower bar charts show % chimerism contribution of mTOR$^{\Delta APC}$-derived cells in control (CD11c^{-}) and CD11c^{+} (red) populations. The *cDC* and *MigDC* abbreviations refer to classical DCs (Mhc-II^{int}) and migratory DCs (Mhc-II^{hi}) respectively. WAT refers to white adipose tissue, LI-LP refers to large intestinal lamina propria, MesLN refers to mesenteric LNs. Bar charts show mean ± SEM, data represents ≥2 independent experiments.

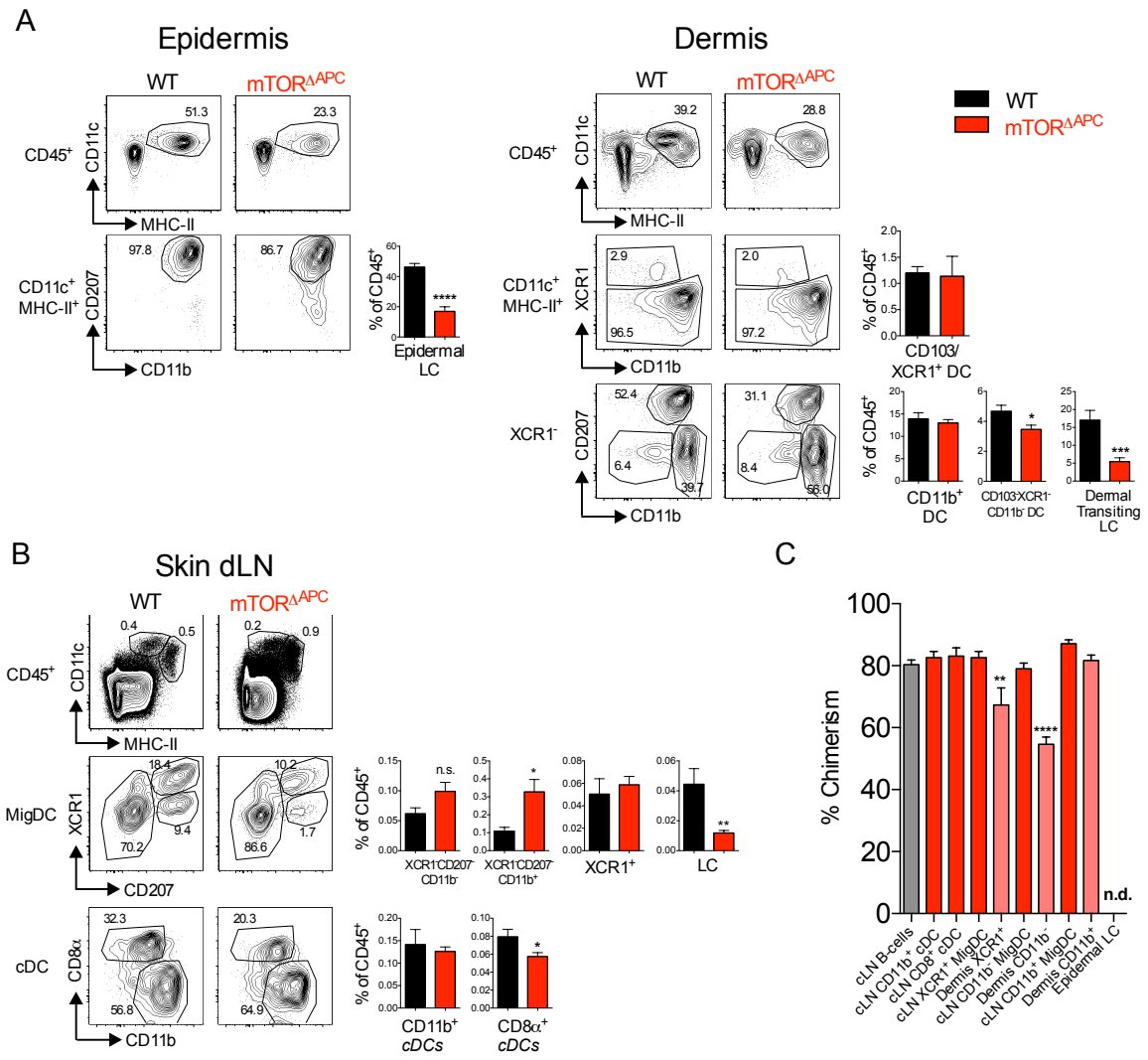

Fig. S3. mTOR is critical to maintain homeostasis of skin-derived DCs.

Single cell suspensions from (**A**) epidermis, dermis and (**B**) skin draining lymph node from WT (Black) or mTOR$^{\Delta APC}$ (red) mice were analyzed by flow cytometry. Contour plots show representative phenotypes and bar charts show pooled frequencies of indicated populations. (**C**) Mixed bone marrow chimeras were established by mixing mTOR$^{\Delta APC}$ (CD45.2) and B6 CD45.1 BM cells (3:1 ratio), and transferring them to B6 CD45.1$^+$/CD45.2$^+$ hosts. Chimeras were analyzed by flow cytometry. The bar chart shows frequency of chimerism contributed by mTOR$^{\Delta APC}$ cells to indicated control CD11c$^-$ (grey), cutaneous LN DC (red), or dermal DC (salmon) populations. Residual CD45.1$^+$CD45.2$^+$ cells were excluded from the analysis. Epidermal Langerhans cell chimerism was not determined, due to radioresistance of this population. Bar charts show mean ± SEM, data represents ≥2 independent experiments.

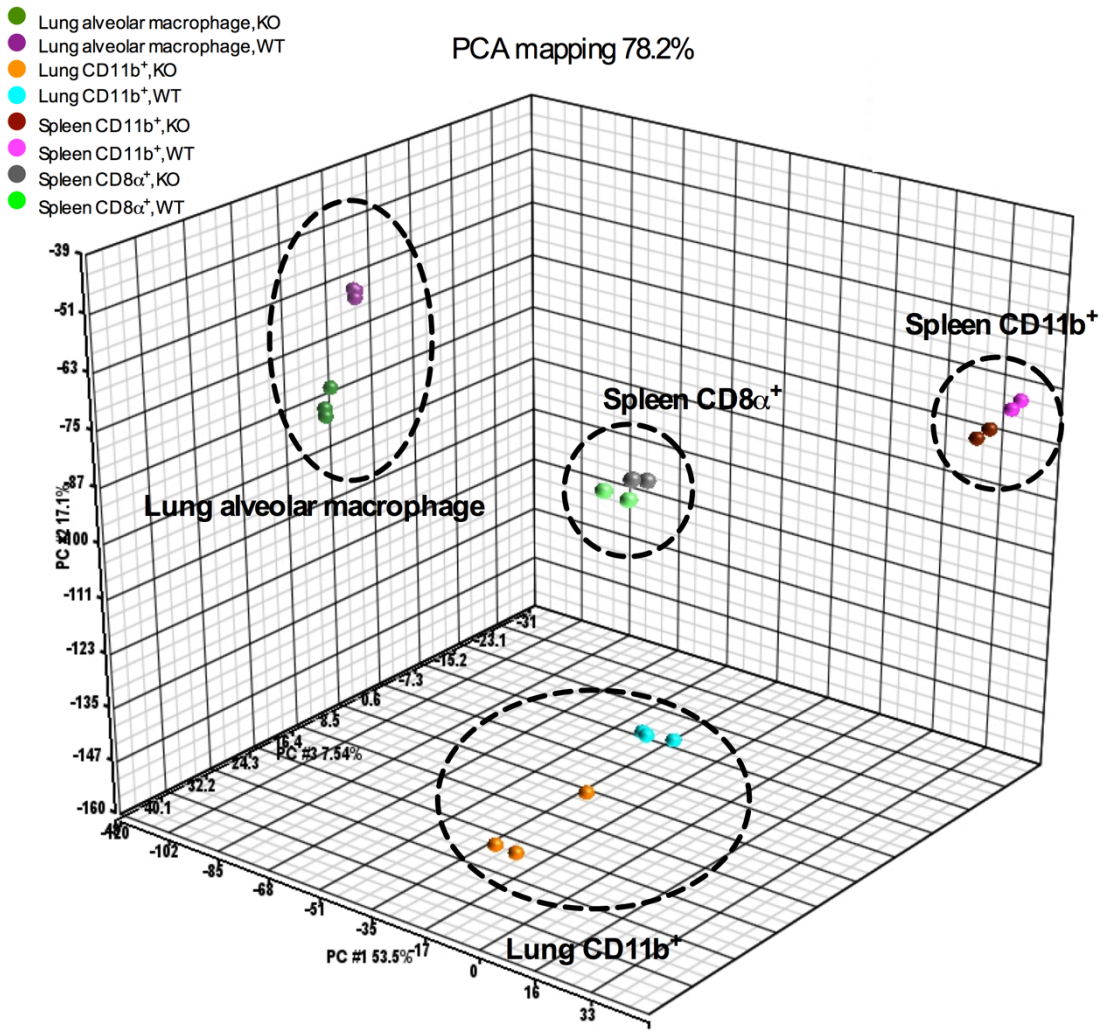

Fig. S4. Loss of cellular identity of lung DCs and AM from mTOR$^{\Delta APC}$ mice.

Transcriptomes of indicated WT and mTOR$^{\Delta APC}$ populations were analyzed by RNA-seq. Unfiltered DESeq2 normalized reads were subjected to PCA analysis. Scatter plot shows principle components 1-3 of indicated APC subsets.

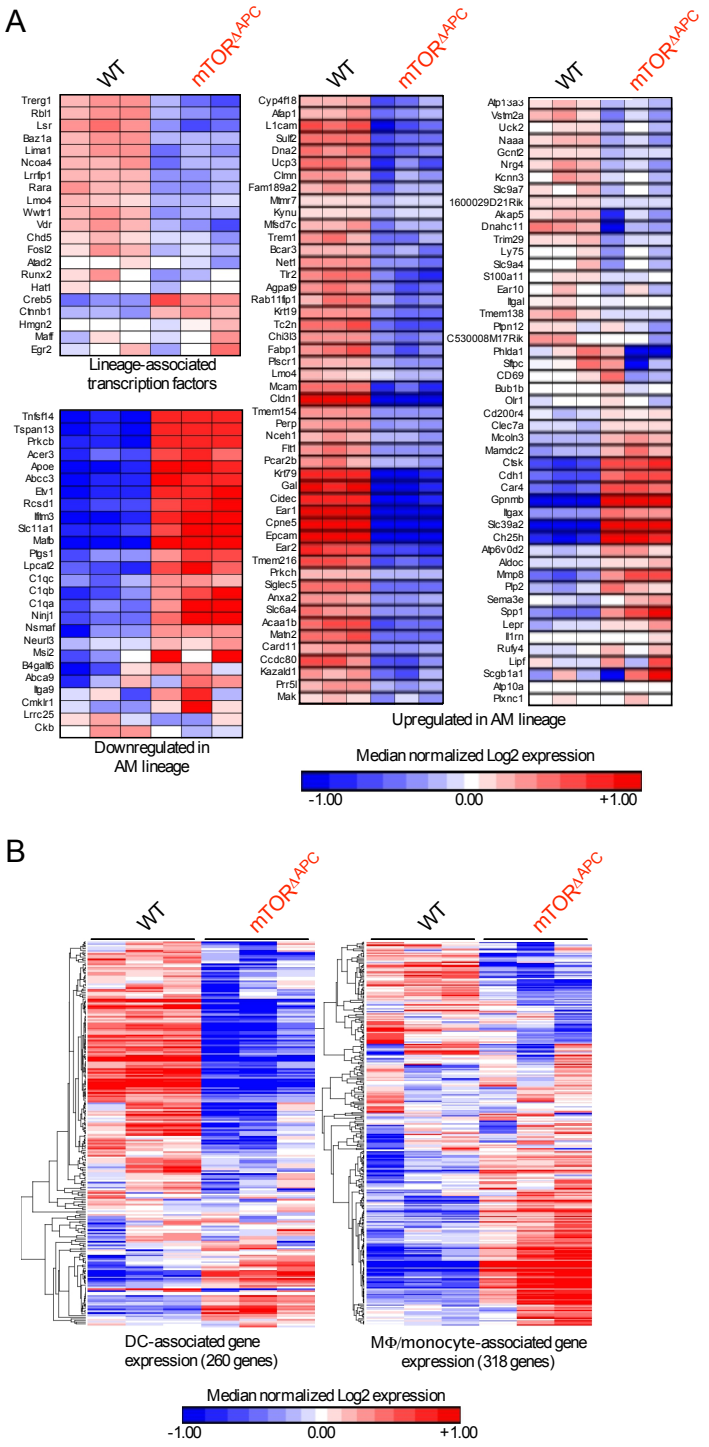

Fig. S5. Gene expression profiles are altered in mTOR$^{\Delta APC}$ lung APCs

(**A**) AMs were purified and analyzed by RNA-seq. Heat maps show expression of transcription factors that are associated with AMs, genes upregulated in AM, and genes downregulated in AMs relative to other myeloid subsets, as defined by Gauthier et al. (*22*) (**B**) Lung classical CD11b^{+} DCs were purified and analyzed by RNA-seq. Heat maps show expression of classical DC-associated genes and macrophage/monocyte-associated

genes, as defined by Schlitzer et al. (*23*). Heat map color intensity shows gene expression relative to the median value across samples (n=3).

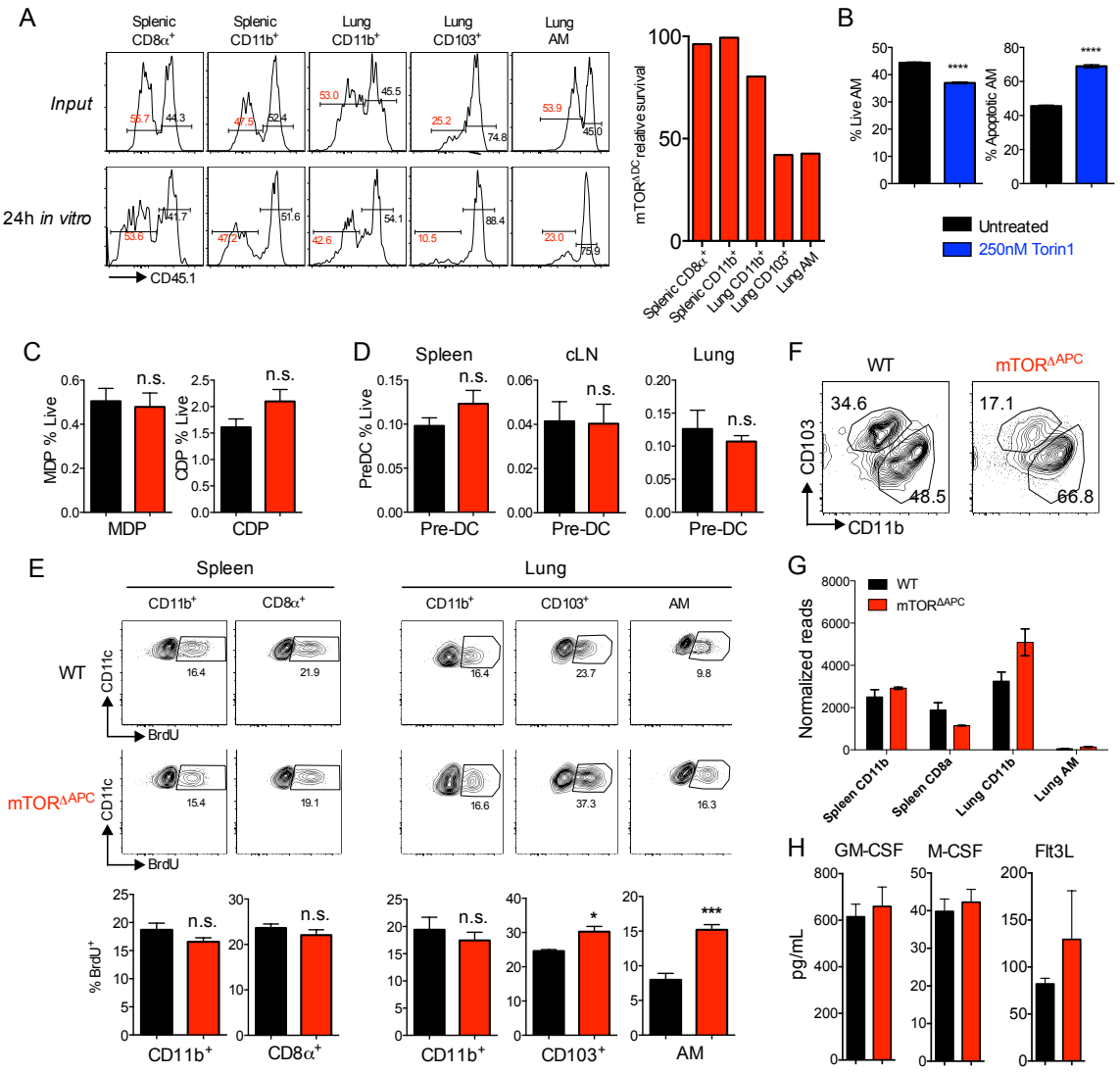

Fig. S6. mTOR deficiency results in elevated death of lung APCs.

(**A**) APCs from mTOR$^{\Delta APC}$ (CD45.1^{-}) and WT control (CD45.1^{+}) were FACS purified and co-cultured for 24h. Histograms show CD45.1^{-} and CD45.1^{+} input frequencies and frequencies at 24h in representative cultures. The bar chart shows ratio of input to output frequency of mTOR$^{\Delta APC}$ cells from the representative plots. (**B**) WT AMs were cultured with the mTOR kinase inhibitor Torin1 for 24h. Cell viability was determined with L/D Aqua®. BM, spleen, cLN and lung from WT (Black) or mTOR$^{\Delta APC}$ (red) mice was examined by flow cytometry. (C) Bar charts show Macrophage/DC progenitor (MDP) and common DC progenitor (CDP) frequencies in BM (*58*). (**D**) Bar charts show Pre-DC frequencies in indicated tissues. (**E**) BrdU incorporation into indicated populations after 2d of labeling *in vivo*. (**F**) Contour plots show CD11c^{+}Mhc-II^{+} DCs from mediastinal lymph node of indicated strains. (**G**) mRNA expression of CCR7 in indicated DC subsets as measured by RNA-seq. (**H**) Measurement of DC homeostatic cytokines in aqueous lung extract by ELISA. Data represent ≥2 independent experiments.

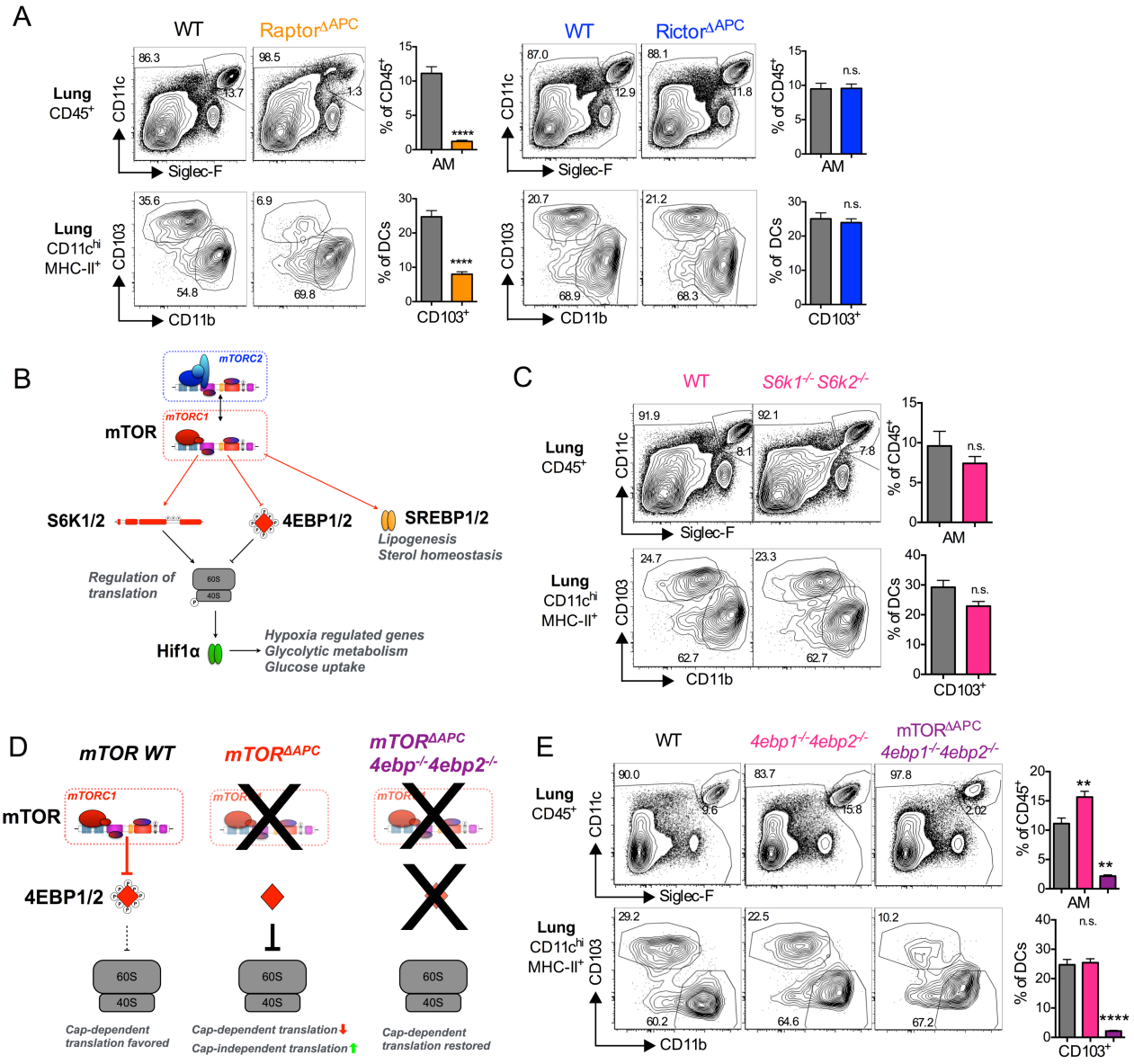

Fig. S7. Lung APC homeostasis is mTORC1-dependent but does not require mTOR-dependent translational regulators S6K1/2 and 4ebp1/2.

Lung preparations from indicated strains were analyzed by flow cytometry. (**A**) Raptor$^{\Delta APC}$ but not Rictor$^{\Delta APC}$ mice exhibit defects in lung APC homeostasis. (**B**) Schematic depicting key signaling events downstream of mTORC1. (**C**) *S6k1*$^{-/-}$*S6k2*$^{-/-}$ mice (pink) do not exhibit defects in lung APC homeostasis. (**D**) Schematic depicting the effects of mTOR deficiency and mTOR/4EBP1/2 deficiency on downstream Cap-dependent translation. (**E**) *4ebp1*$^{-/-}$*4ebp2*$^{-/-}$ (pink) or mTOR$^{\Delta APC}$*4ebp1*$^{-/-}$*4ebp2*$^{-/-}$ mice (purple) do not exhibit defects in lung APC homeostasis. Data represents ≥2 independent experiments, n≥3 mice.

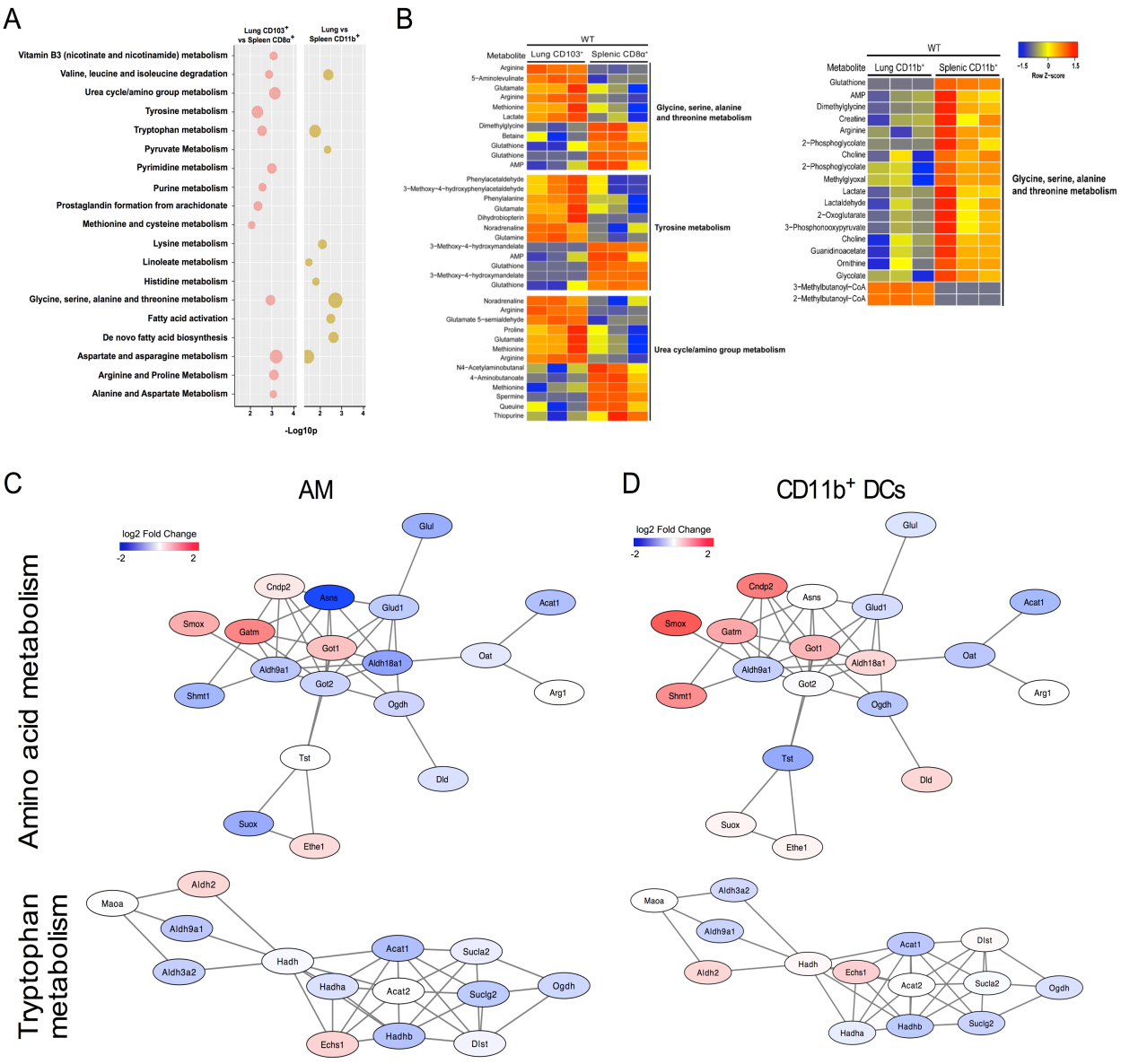

Fig. S8. Metabolic differences between splenic and lung DC populations.

Cellular metabolomic profiling was performed on indicated FACS purified populations from WT or mTOR$^{\Delta APC}$ mice. (**A**) Pathway analysis of metabolic differences between equivalent lung and splenic DC populations. Dot size corresponds to the relative number of differentially expressed metabolites. (**B**) Heat maps of selected differentially expressed metabolite pathways related to amino acid metabolism. The metabolite labels are based on tentative annotation from the mummichog software, and include multiple adducts. (**C-D**) Transcriptional network map of amino acid metabolism and tryptophan metabolism genes for (**C**) AM, and (**D**) CD11b^{+} DC populations.

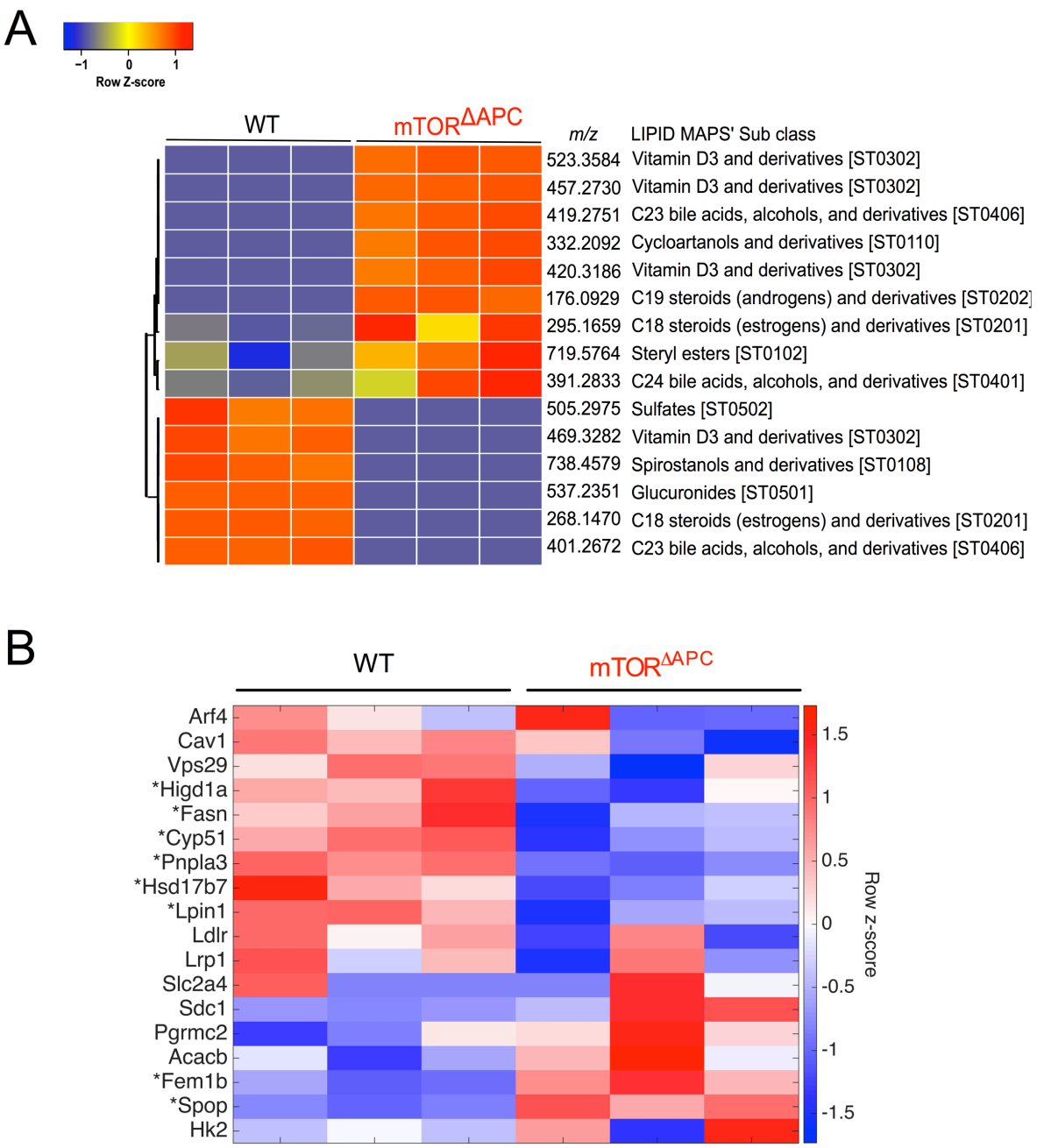

Fig. S9. mTOR$^{\Delta APC}$ alveolar macrophages exhibit alterations in lipid metabolism associated with perturbed Srebp1/2-dependent gene signatures.

Metabolomic and transcriptomic profiles from WT and mTOR$^{\Delta APC}$ AMs were analyzed. (**A**) Heat map shows differential abundance of sterol lipid metabolites, based on tentative annotations by accurate *m/z* matching to LIPID MAPS database. (**B**) Heat map showing expression of Srebp1 target genes. Differentially expressed genes ($p<0.05$, t-test) are denoted by *.

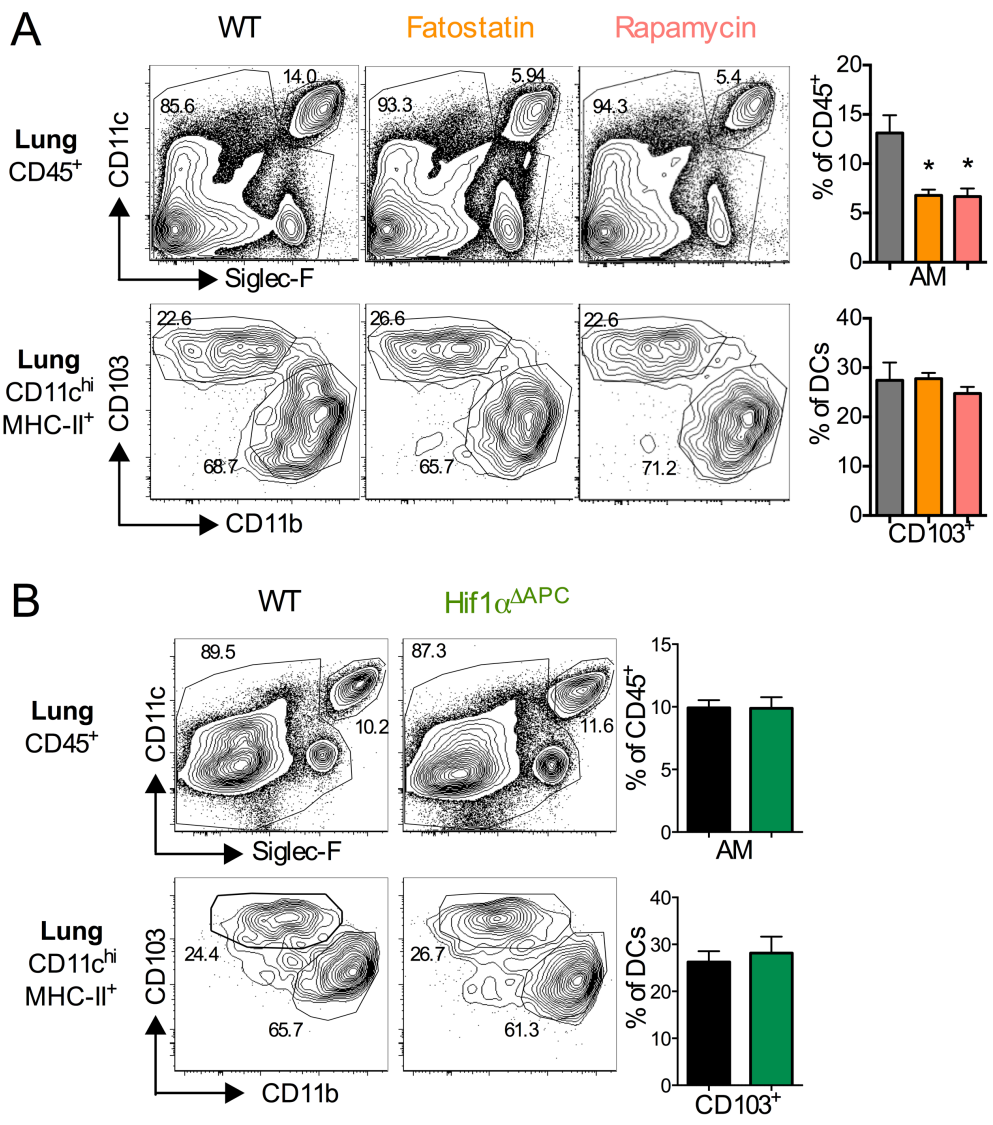

Fig. S10. AM homeostasis is Srebp-dependent but Hif1α-independent.

(**A**) Administration of the Srebp1/2 inhibitor fatostatin (orange), or the mTORC1 inhibitor rapamycin (salmon) disrupts AM homeostasis in lung. (**B**) Hif1α$^{\Delta APC}$ mice (green) do not exhibit defects in lung APC homeostasis. Data represents ≥2 independent experiments, n≥3 mice.

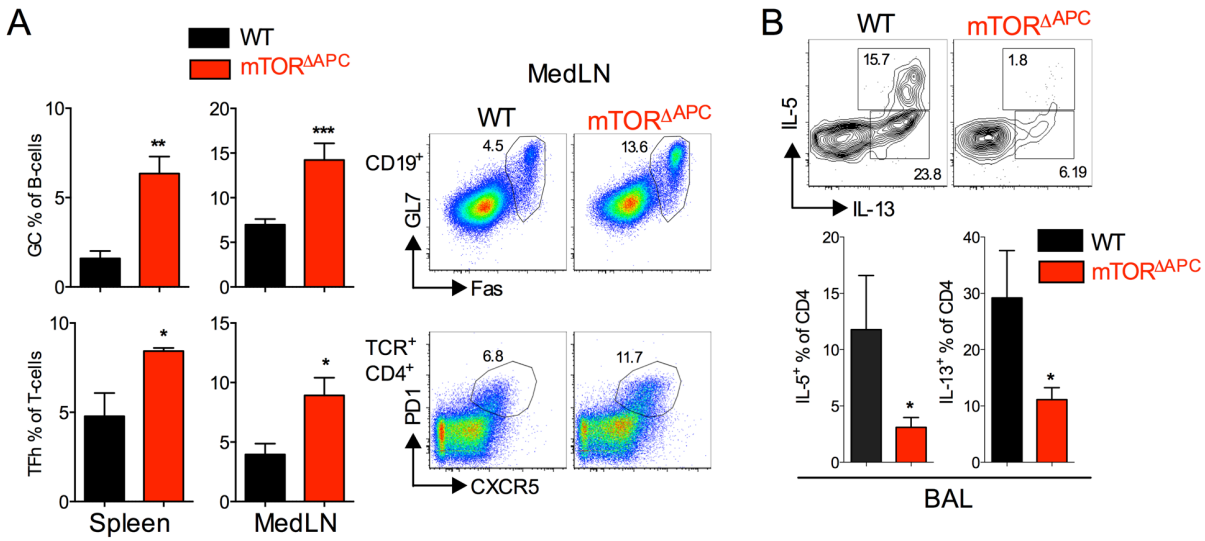

Fig. S11. Allergy in mTOR$^{\Delta APC}$ mice is typified by enhanced B-cell response but reduced Th2 cytokine production.

House dust mite (HDM) extract was administered to WT (black) or mTOR$^{\Delta APC}$ mice (red). (**A**) Bar charts show B-cell germinal center (GC) and T-follicular helper (TFh) frequency. Pseudo-color plots show representative flow cytometric data. (**B**) Bar charts show frequency of CD4^{+}IL-5^{+} and CD4^{+}IL-13^{+} T-cells in BAL. Contour plots show representative flow cytometric data. Data represents ≥3 independent experiments.

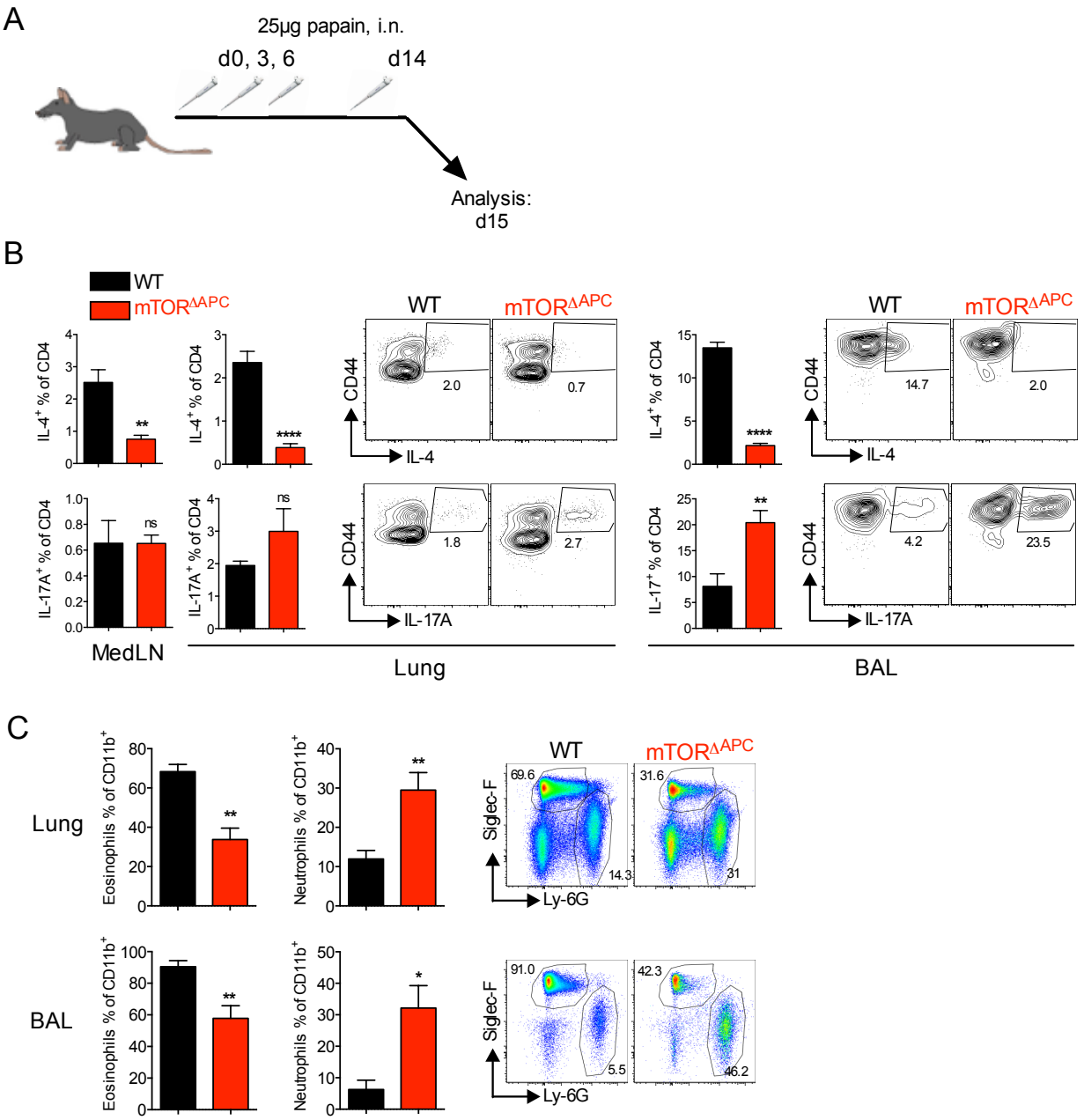

Fig. S12. Th17/neutrophilia in a papain induced allergy model.

Allergy was induced in mTOR$^{\Delta APC}$ or controls by administration of papain i.n. (**A**) Diagram shows the vaccination and analysis schedule. (**B**) Bar charts show frequencies of CD4$^+$IL-4$^+$ Th2 cells or CD4$^+$IL-17A$^+$ Th17 cells in indicated organs after restimulation with PMA and ionomycin. Contour plots show representative flow cytometric data. (**C**) Bar charts show frequencies of CD11b$^+$Siglec-F$^+$ Eosinophils or CD11b$^+$Ly-6G$^+$ neutrophils. Pseudo-color plots show representative flow cytometric data. Bar charts show mean ± SEM, data represent two independent experiments.

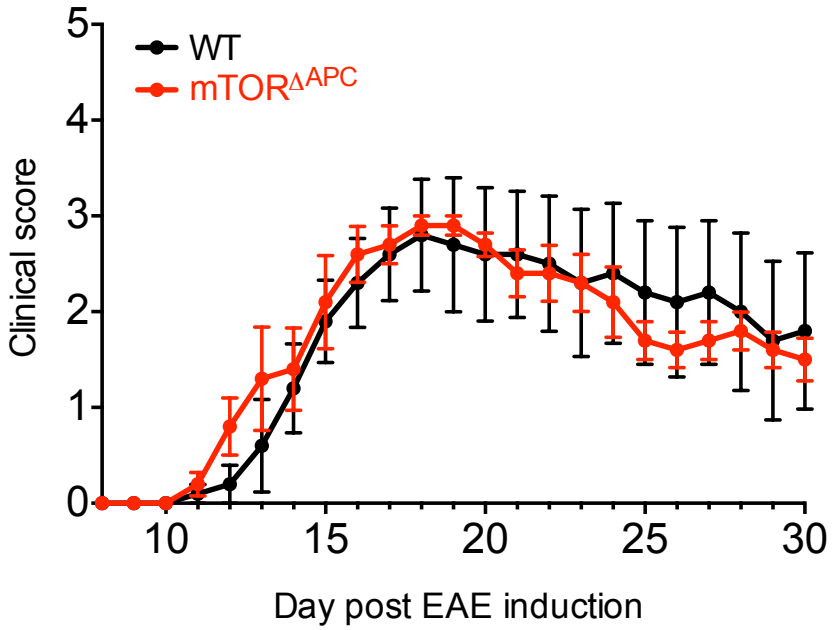

Fig. S13. mTOR deficiency in APCs does not impact induction or progression of disease in an experimental autoimmune encephalomyelitis (EAE) model.

EAE was induced in WT and mTOR$^{\Delta APC}$ mice (n=5/group) and clinical disease score was monitored over a 30 day period.

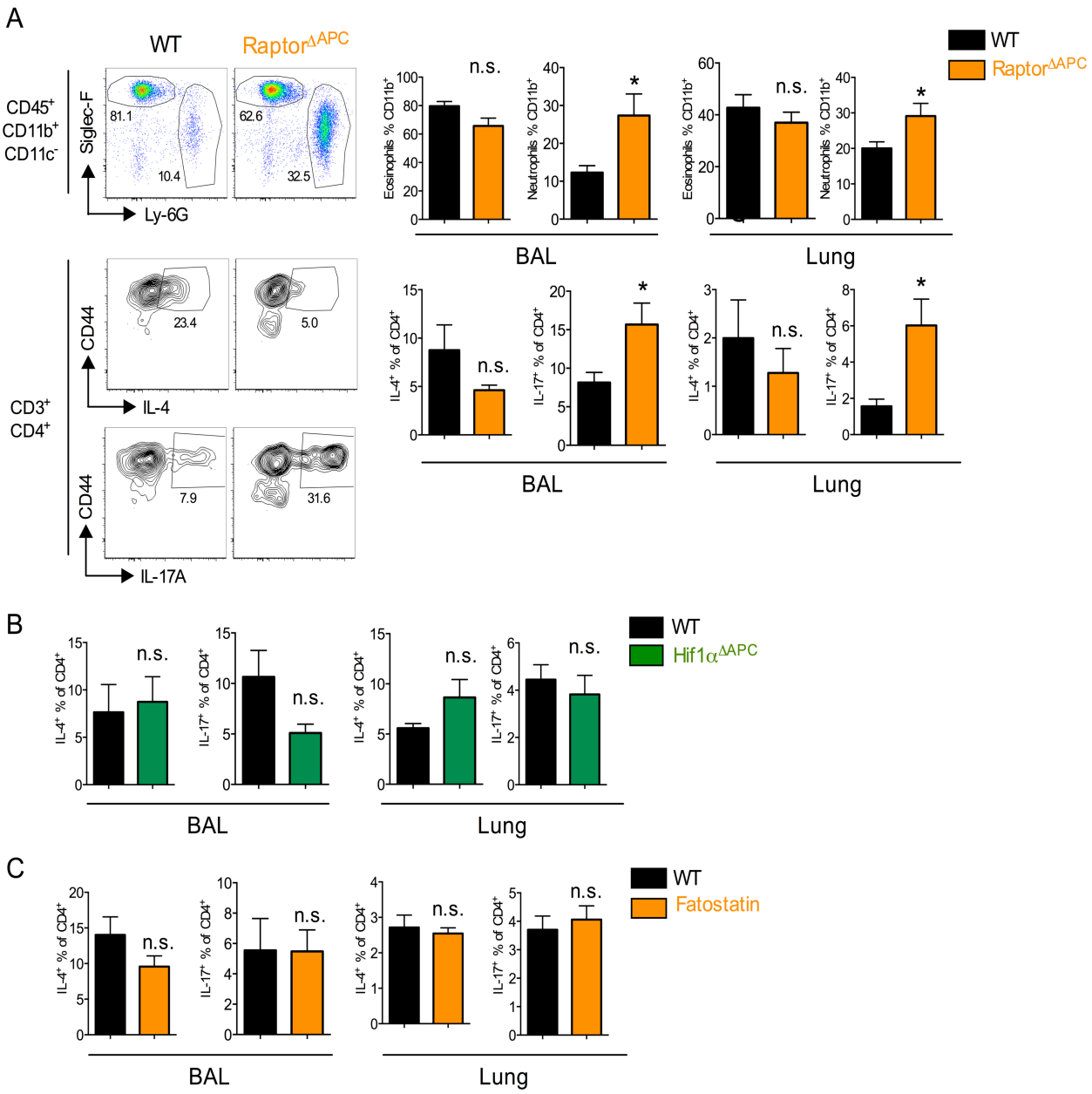

Fig. S14. Th17 lung allergy is dependent on mTORC1 signaling.

Allergy was induced for three weeks in (**A**) Raptor$^{\Delta APC}$ (**B**) Hif1α$^{\Delta APC}$ strains, or (**C**) Fatostatin treated WT mice. (**A**) Pseudocolor plots show expression of Siglec-F versus Ly6-G in BAL cells. Contour plots show expression of CD44 versus IL-4 or IL-17A cytokines in BAL cells. (**A-C**) Bar charts show the frequency of indicated populations for indicated experimental groups. Data represents two experiments, n≥5 per experimental group.

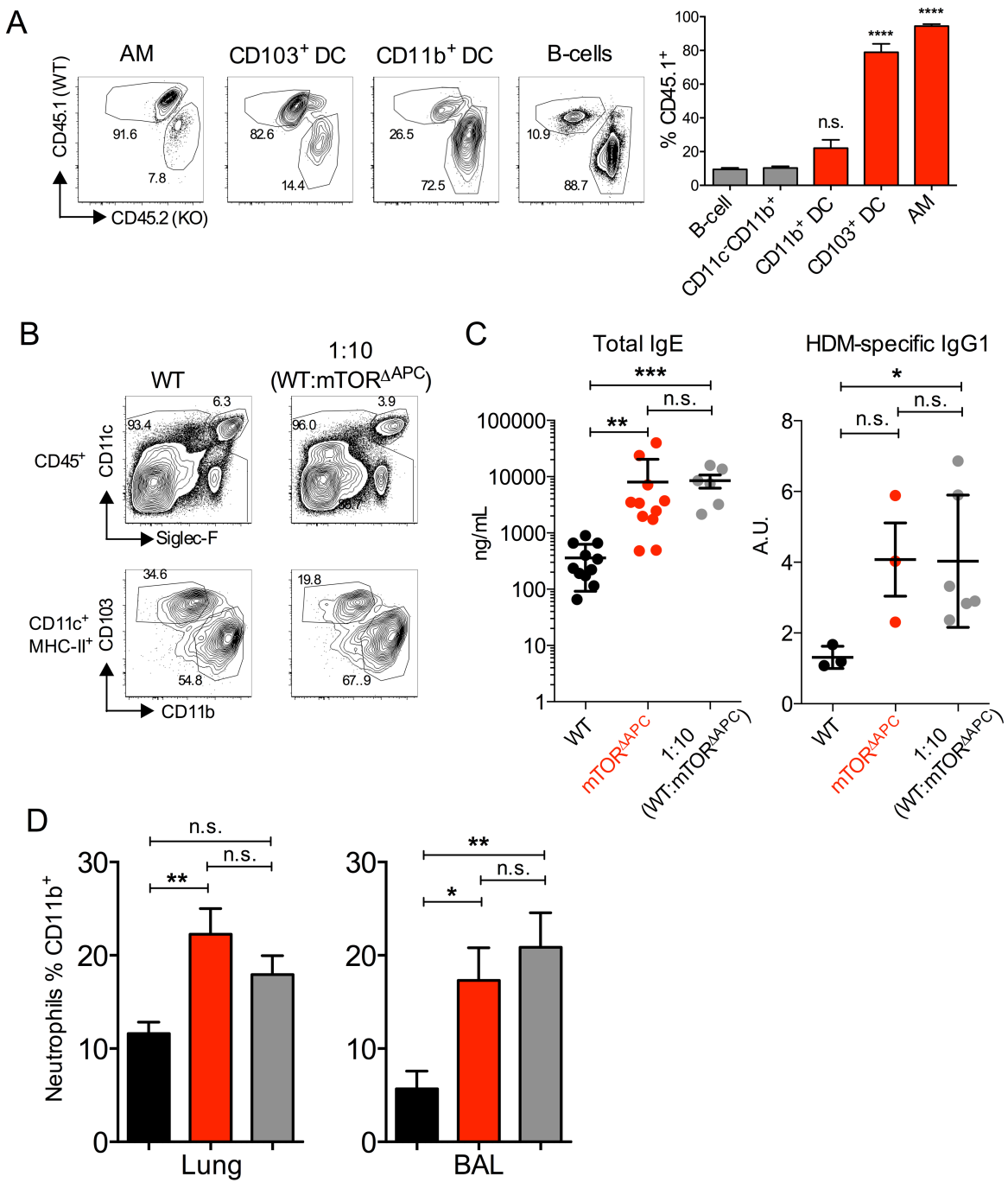

Fig. S15. Neutrophilic allergy in mTOR$^{\Delta APC}$ mice cannot be rescued by restoring homeostatically deficient APC populations.

Mixed bone marrow chimeras were established by mixing mTOR$^{\Delta APC}$ (CD45.2) and B6 CD45.1 BM cells (1:10 ratio), and transferring them to B6 CD45.1^{+}/CD45.2^{+} hosts. (**A-B**) Chimeric mice were analyzed in the steady-state or (**C-D**) following chronic HDM administration. (**A**) Bar chart shows % chimerism contribution of mTOR$^{\Delta APC}$-derived cells in control (CD11c^{-}) and CD11c^{+} (red) populations. Contour plots show representative data. (**B**) Contour plots show restoration of CD11c^{+}Siglec-F^{+} alveolar

macrophage and $CD11c^{+}Mhc\text{-}II^{+}CD103^{+}$ DC populations. (**C**) Scatter plots show HDM-induced serum antibody titers from indicated groups. (**D**) Bar charts show frequencies of neutrophils in lung and BAL. Bar charts represent mean ± SEM, data is pooled from two independent experiments.

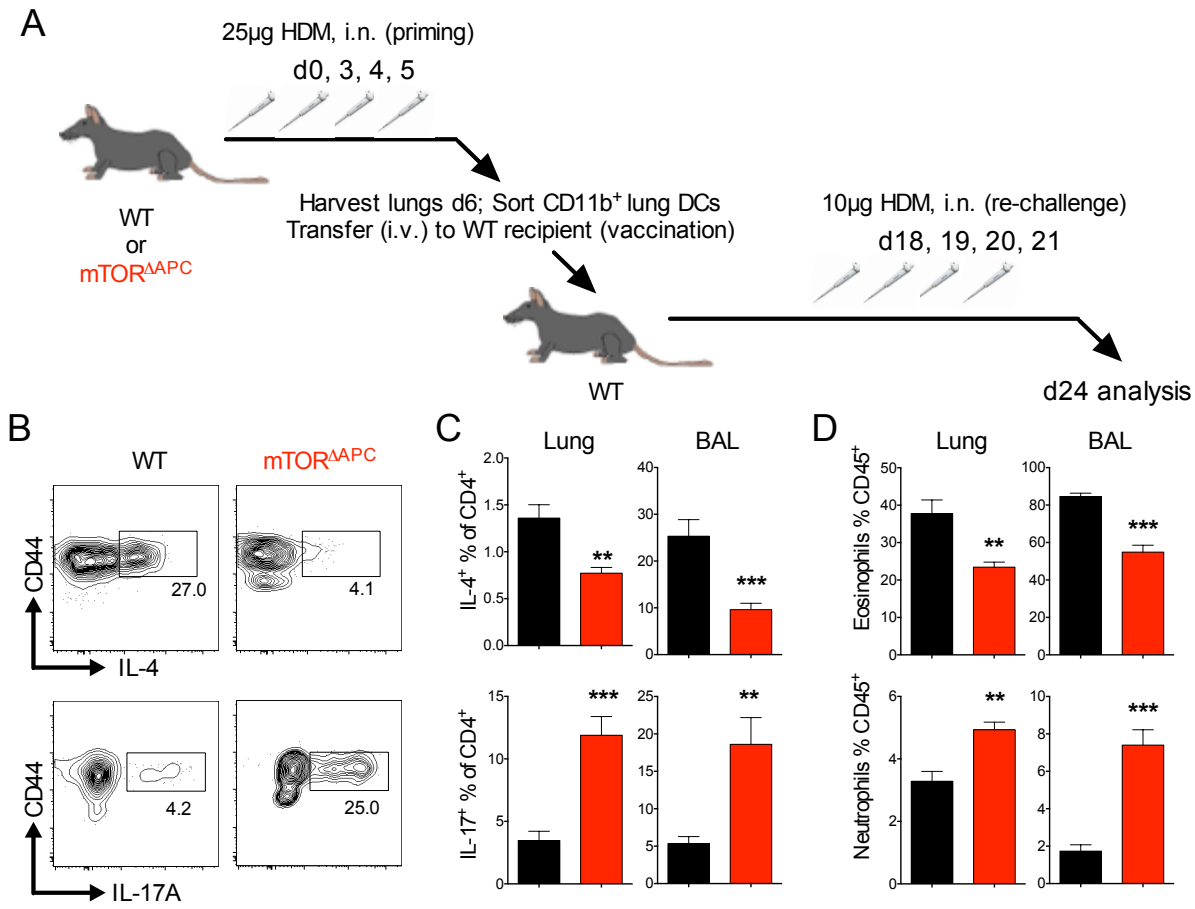

Fig. S16. Th17/Neutrophilic allergy is CD11b$^+$ DC-dependent.

(**A**) Schematic shows DC vaccination protocol to transfer Th17/neutrophilic allergy. HDM was administered to WT (black) or mTOR$^{\Delta APC}$ (red) mice to prime immunity. On day 6, CD11b$^+$ DCs were sorted from lung and transferred to WT recipients. Recipients were re-challenged with 10ug HDM, lung and BAL was analysed by flow cytometry on d24. (**B**) Representative BAL contour plots and (**C**) bar charts of pooled data from lung and BAL showing IL-4$^+$ and IL-17$^+$ T-cells in lung or BAL. **(D)** Bar charts show frequencies of eosinophils and neutrophils in lung and BAL. Data represents two independent experiments.

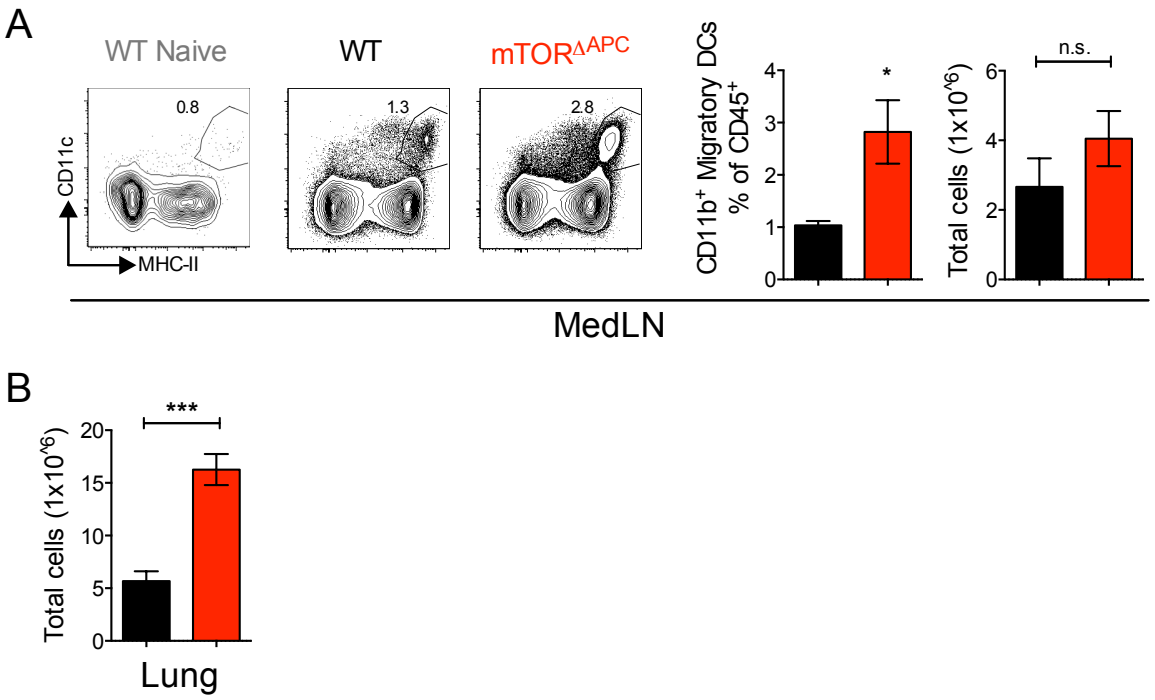

Fig. S17. mTOR$^{\Delta APC}$ exhibit sensitivity to acute allergy challenge.

75µg HDM was administered i.t. to WT and mTOR$^{\Delta APC}$ mice, on d0 and d2. Lungs were analyzed by on d3. (**A**) Contour plots and left bar chart show frequency of migratory DCs in MedLN. Right bar chart shows total cell counts from MedLN. (**B**) Bar chart shows total cell counts from lung.

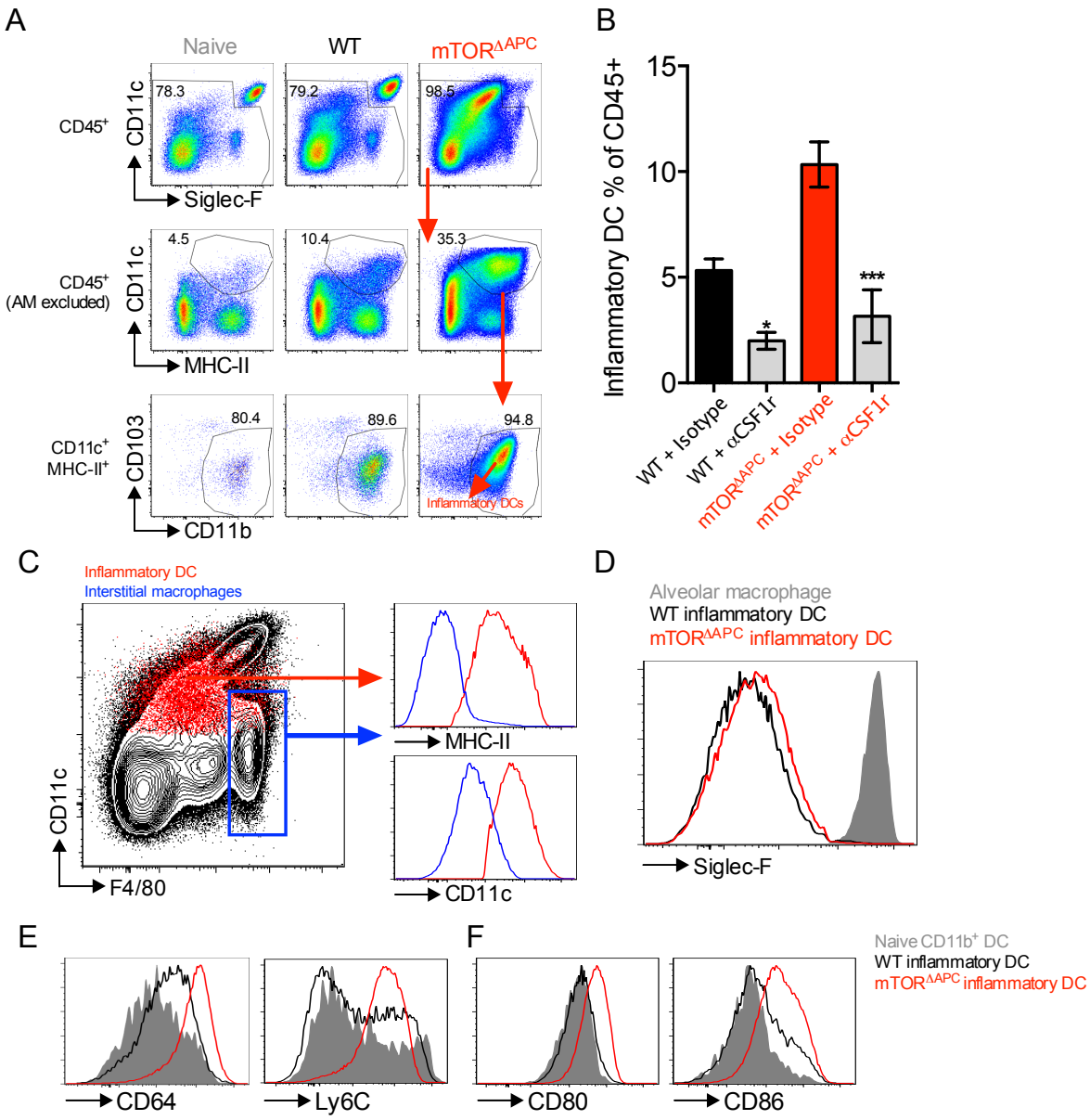

Fig. S18. CSF1r-dependent inflammatory DCs differentiate in lung following HDM stimulus.

(**A**) WT or mTOR$^{\Delta APC}$ mice were treated for a short-term with HDM on d0 and d2, and analyzed on d3 along with WT naïve controls by flow cytometry. Pseudo-color plots show hierarchical gating strategy to identify Siglec-F^{-} CD11c^{+}Mhc-II^{+}CD103^{-}CD11b^{+} DCs arising under allergic inflammatory conditions. The inflammatory DC gate used for subsequent analyses is indicated. (**B**) WT or mTOR$^{\Delta APC}$ mice were chronically treated with HDM for 3 weeks. Bar chart shows the frequency of inflammatory DCs. (**C**) Contour plot shows expression of CD11c and F4/80 on total CD45^{+} cells from short-term HDM treated WT mice (3d intratracheal HDM administration). Red overlay shows the phenotype of inflammatory DCs, identified based on the gating strategy in (**A**). The blue gate shows the distinction of inflammatory DCs from F4/80^{hi}CD11c^{lo} interstitial macrophages. Histograms compare Mhc-II and CD11c expression on interstitial

macrophages (blue) and inflammatory DCs (red). (**D**) Histograms show expression of Siglec-F on indicated APC populations. (**E**) Histograms show expression of CD64 and Ly6C and (**F**) CD80 and CD86 on lung inflammatory DCs from short-term HDM treated WT and $mTOR^{\Delta APC}$ as compared to WT mediastinal migratory $CD11b^{+}$ DCs. Data represents ≥3 independent experiments.

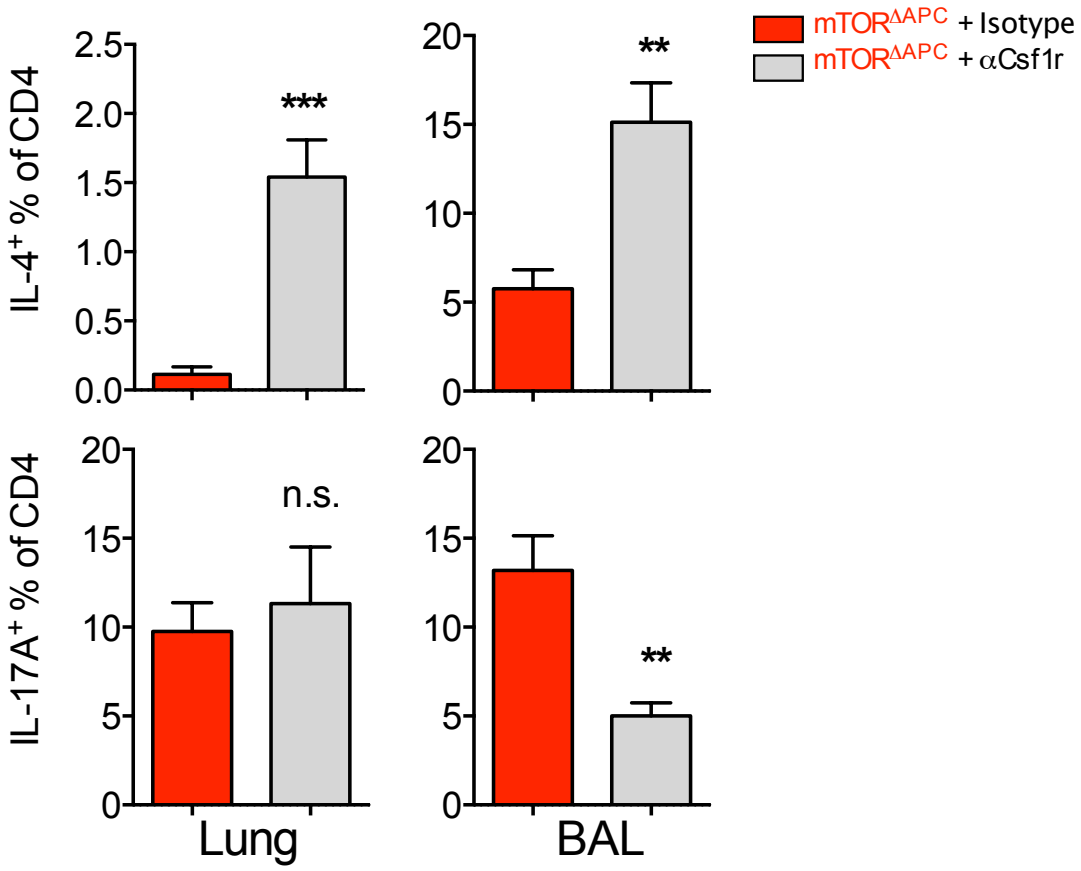

Fig. S19. Blockade of inflammatory DC differentiation inhibits Th17 and restores Th2 polarization in mTOR$^{\Delta APC}$ mice.

Chronic allergic responses were induced with HDM in groups of mTOR$^{\Delta APC}$ mice for three weeks. Mice were constitutively treated with Csf1r or isotype control neutralizing antibodies. Bar charts show frequency of Th2 (IL-4^{+}) and Th17 (IL-17A^{+}) cells in indicated tissues, and indicate mean ± SEM. Data is representative of two independent experiments.

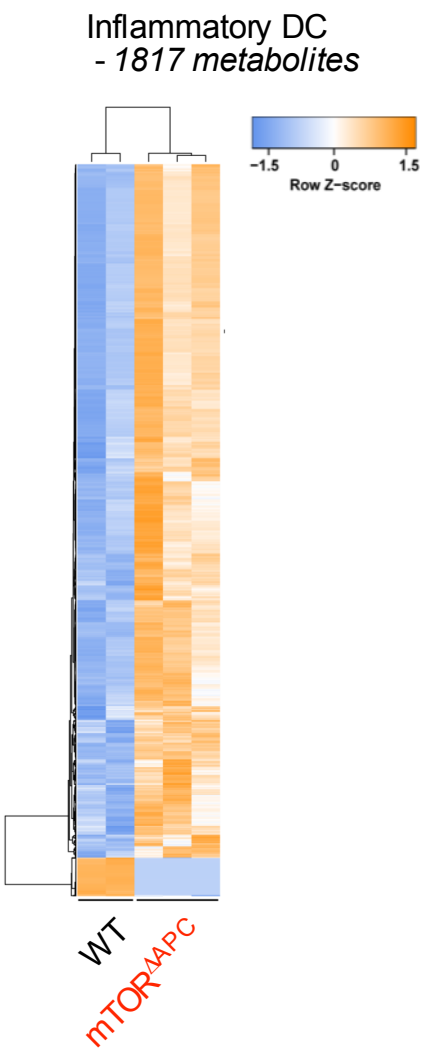

Fig. S20. Inflammatory DCs from mTOR$^{\Delta APC}$ mice exhibit distinct metabolic features.

75µg HDM was administered i.t. to WT and mTOR$^{\Delta APC}$ mice, on d0 and day 2. Lungs were analyzed by on d3. Heat map shows differential abundance of metabolic features in WT and mTOR$^{\Delta APC}$ inflammatory DCs.

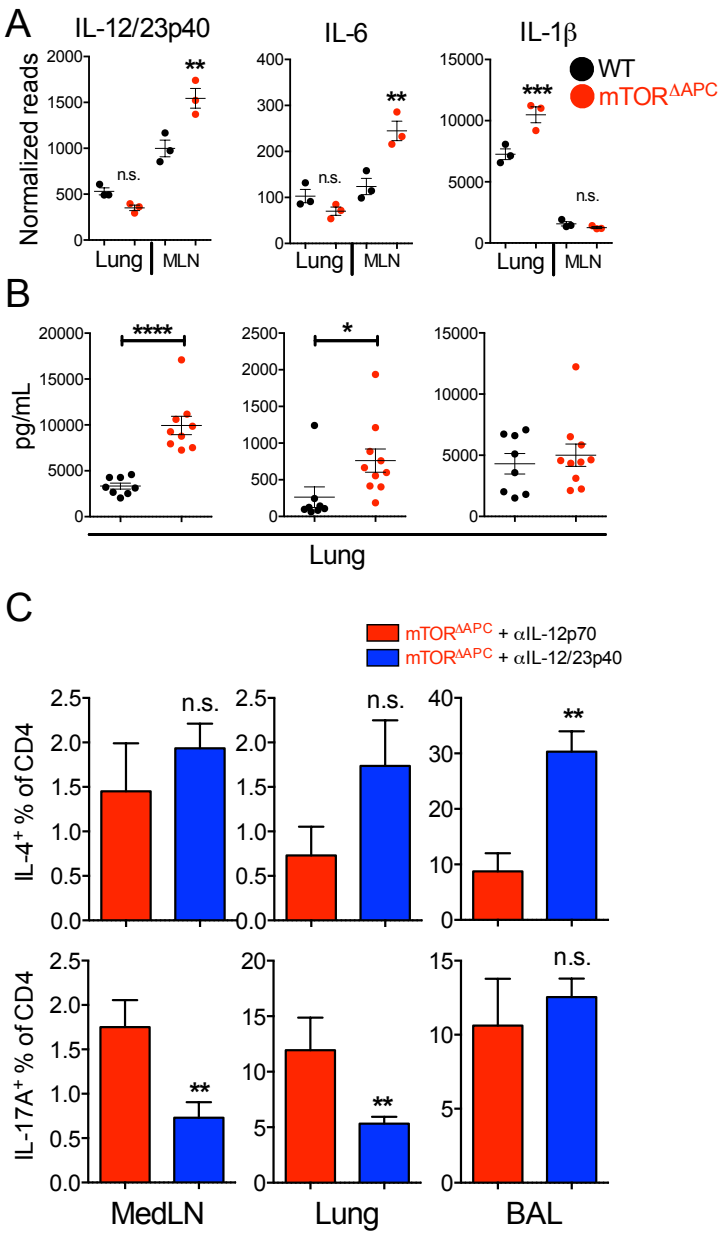

Fig. S21. Blockade of IL-23 inhibits Th17 and restores Th2 polarization in mTOR$^{\Delta APC}$ mice.

(**A**-**B**) 75µg HDM was administered i.t. to WT and mTOR$^{\Delta APC}$ mice, on d0 and d2. Lungs were analyzed by on d3. (**A**) Scatter bar charts show expression of key cytokines from lung inflammatory DC and mediastinal lymph node resident classical CD11b^{+} DC populations measured by RNA-seq after short-term HDM administration.(**B**) Scatter plots show expression of cytokines in lung homogenate as measured by ELISA after short-term HDM administration. (**C**) Mice were constitutively treated with IL-12p70 control (red) or IL12/23p40 (blue) neutralizing antibodies for three weeks. Bar charts show frequency of Th2 (IL-4^{+}) and Th17 (IL-17A^{+}) cells in indicated tissues, and indicate mean ± SEM. Data is representative of two independent experiments.

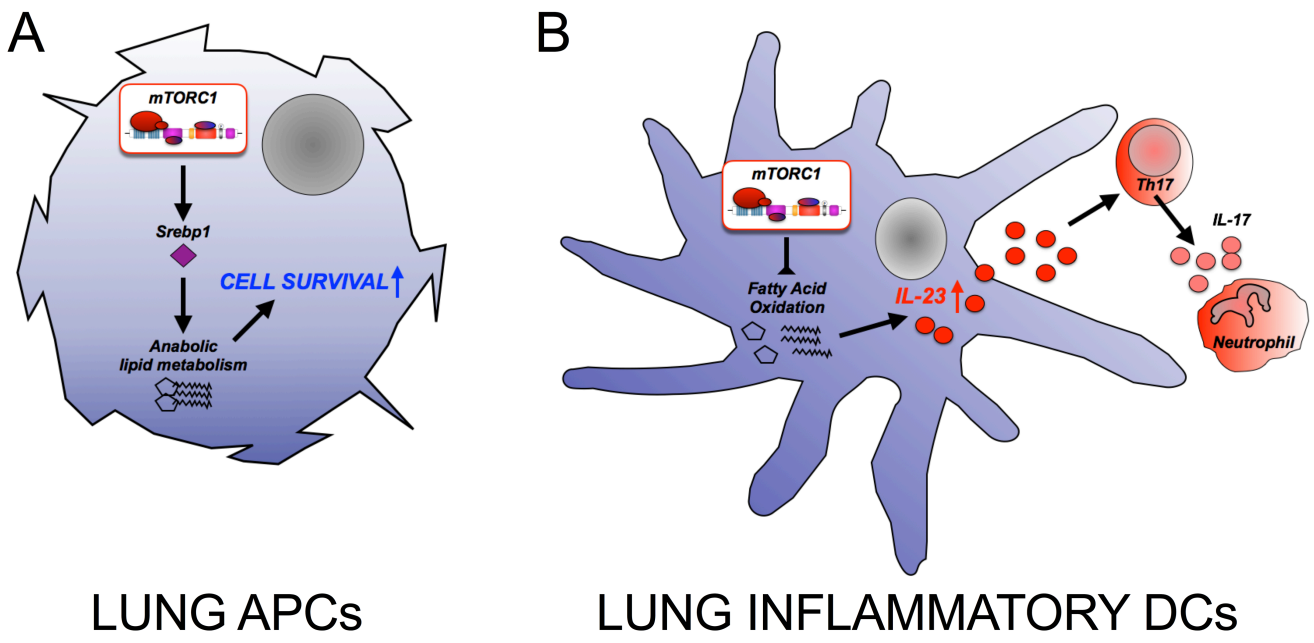

Fig. S22. Model of mTOR-dependent functions in lung APCs.

(**A**) In the steady-state mTOR signaling is required to establish homeostatic accumulation of APCs promoting cell survival. Moreover, in AMs, our study additionally revealed a critical requirement for the anabolic lipid metabolic regulator Srebp1 in accumulation of this subset. Impaired APC accumulation in mTOR$^{\Delta APC}$ mice resulted in immuno-deficiencies that reduced antiviral responses, and perturbed AM functions resulting in acquisition of pulmonary alveolar proteinosis. (**B**) During allergy, mTOR restricts catabolic metabolism, a rate-limiting step in DC activation and cytokine production. In the absence of mTOR signaling, inflammatory DCs exhibit pronounced fatty acid oxidation and induce Th17/neutrophilic lung inflammation via an IL-23-dependent mechanism.

Table S1.

Antibody	Clone	Flurophore/s	Additional vendor information
BrdU	Not specified	APC	Component of BD Pharmingen BrdU staining kit
CD3	17A2	PE-Cy7, Brilliant Violet™(bv)650	
CD4	RM4-5	bv650, bv711, bv785	
CD8	53 6.7	PerCP, Pacific blue, bv711, bv421	Pacific blue from BD
CD11b	M1/70	bv650	
CD11c	N418	APC, bv421	
CD19	6D5	bv785	
CD44	IM7	bv421	
CD45	30-F11	bv570, bv711	
CD45.1	A20	bv711	
CD45.2	104	FITC	
CD64	X54-5/7.1	PeCy7	
CD80	16-10A1	FITC	
CD86	PO3	FITC, APC	
CD95/Fas	Jo2	PE-CF594	BD horizon
CD103	2E7	FITC, PE	
c-kit (CD117)	2B8	Alexa488	
CSF-1R (CD115)	AFS98	APC	
CXCR5	SPRCL5	Unconjugated primary	
F4/80	BM8	APC	
Flt3	A2F10	PE	
GL7	GL7	FITC	
HSA (CD24)	M1/69	PE, APC	
IFNγ	XMG1.2	FITC	
IL-4	11B11	PE, APC	
IL-12/23p40	C17.8	PE	
IL-17A	TC11-18H10	PE-CF594	
Ly6G	1A8	APC-Cy7	
MHC-II	M5/114.15.2	Alexa700	
mTOR	7C10	Alexa488, Alexa647	Cell signaling technology
PD1 (CD279)	MIH4	PECF594	BD horizon
pDCa (CD317)	927	APC	
Phospho-S6 Ser235/236	D57.2.2E	PE	Cell signaling technology
Phospho-S6 Ser240/244	D68F8	Alexa488	Cell signaling technology
Pro-IL1β	NJTEN3	PE	
Siglec-F	E50-2440	PE, PE-CF594	BD horizon
Sirpα (CD172a)	P84	PE-Cy7, APC	
TCR-β	H57-597	Alexa700	

References

1. E. J. Pearce, B. Everts, Dendritic cell metabolism. *Nat. Rev. Immunol.* **15**, 18–29 (2015). doi:10.1038/nri3771 Medline

2. B. Pulendran, The varieties of immunological experience: Of pathogens, stress, and dendritic cells. *Annu. Rev. Immunol.* **33**, 563–606 (2015). doi:10.1146/annurev-immunol-020711-075049 Medline

3. T. D. Querec, R. S. Akondy, E. K. Lee, W. Cao, H. I. Nakaya, D. Teuwen, A. Pirani, K. Gernert, J. Deng, B. Marzolf, K. Kennedy, H. Wu, S. Bennouna, H. Oluoch, J. Miller, R. Z. Vencio, M. Mulligan, A. Aderem, R. Ahmed, B. Pulendran, Systems biology approach predicts immunogenicity of the yellow fever vaccine in humans. *Nat. Immunol.* **10**, 116–125 (2009). doi:10.1038/ni.1688 Medline

4. R. Ravindran, N. Khan, H. I. Nakaya, S. Li, J. Loebbermann, M. S. Maddur, Y. Park, D. P. Jones, P. Chappert, J. Davoust, D. S. Weiss, H. W. Virgin, D. Ron, B. Pulendran, Vaccine activation of the nutrient sensor GCN2 in dendritic cells enhances antigen presentation. *Science* **343**, 313–317 (2014). doi:10.1126/science.1246829 Medline

5. R. Ravindran, J. Loebbermann, H. I. Nakaya, N. Khan, H. Ma, L. Gama, D. K. Machiah, B. Lawson, P. Hakimpour, Y. C. Wang, S. Li, P. Sharma, R. J. Kaufman, J. Martinez, B. Pulendran, The amino acid sensor GCN2 controls gut inflammation by inhibiting inflammasome activation. *Nature* **531**, 523–527 (2016). doi:10.1038/nature17186 Medline

6. N. Sukhbaatar, M. Hengstschläger, T. Weichhart, mTOR-mediated regulation of dendritic cell differentiation and function. *Trends Immunol.* **37**, 778–789 (2016). doi:10.1016/j.it.2016.08.009 Medline

7. M. Laplante, D. M. Sabatini, mTOR signaling in growth control and disease. *Cell* **149**, 274–293 (2012). doi:10.1016/j.cell.2012.03.017 Medline

8. F. J. Dumont, M. J. Staruch, S. L. Koprak, M. R. Melino, N. H. Sigal, Distinct mechanisms of suppression of murine T cell activation by the related macrolides FK-506 and rapamycin. *J. Immunol.* **144**, 251–258 (1990). Medline

9. R. Keating, T. Hertz, M. Wehenkel, T. L. Harris, B. A. Edwards, J. L. McClaren, S. A. Brown, S. Surman, Z. S. Wilson, P. Bradley, J. Hurwitz, H. Chi, P. C. Doherty, P. G. Thomas, M. A. McGargill, The kinase mTOR modulates the antibody response to provide cross-protective immunity to lethal infection with influenza virus. *Nat. Immunol.* **14**, 1266–1276 (2013). doi:10.1038/ni.2741 Medline

10. K. Araki, A. P. Turner, V. O. Shaffer, S. Gangappa, S. A. Keller, M. F. Bachmann, C. P. Larsen, R. Ahmed, mTOR regulates memory CD8 T-cell differentiation. *Nature* **460**, 108–112 (2009). doi:10.1038/nature08155 Medline

11. R. Colina, M. Costa-Mattioli, R. J. O. Dowling, M. Jaramillo, L.-H. Tai, C. J. Breitbach, Y. Martineau, O. Larsson, L. Rong, Y. V. Svitkin, A. P. Makrigiannis, J. C. Bell, N. Sonenberg, Translational control of the innate immune response through IRF-7. *Nature* **452**, 323–328 (2008). doi:10.1038/nature06730 Medline

12. W. Cao, S. Manicassamy, H. Tang, S. P. Kasturi, A. Pirani, N. Murthy, B. Pulendran, Toll-like receptor-mediated induction of type I interferon in plasmacytoid dendritic cells requires the rapamycin-sensitive PI(3)K-mTOR-p70S6K pathway. *Nat. Immunol.* **9**, 1157–1164 (2008). doi:10.1038/ni.1645 Medline

13. T. Weichhart, G. Costantino, M. Poglitsch, M. Rosner, M. Zeyda, K. M. Stuhlmeier, T. Kolbe, T. M. Stulnig, W. H. Hörl, M. Hengstschläger, M. Müller, M. D. Säemann, The TSC-mTOR signaling pathway regulates the innate inflammatory response. *Immunity* **29**, 565–577 (2008). doi:10.1016/j.immuni.2008.08.012 Medline

14. T. Sathaliyawala, W. E. O'Gorman, M. Greter, M. Bogunovic, V. Konjufca, Z. E. Hou, G. P. Nolan, M. J. Miller, M. Merad, B. Reizis, Mammalian target of rapamycin controls dendritic cell development downstream of Flt3 ligand signaling. *Immunity* **33**, 597–606 (2010). doi:10.1016/j.immuni.2010.09.012 Medline

15. B. Kellersch, T. Brocker, Langerhans cell homeostasis in mice is dependent on mTORC1 but not mTORC2 function. *Blood* **121**, 298–307 (2013). doi:10.1182/blood-2012-06-439786 Medline

16. S. P. Nobs, C. Schneider, M. G. Dietrich, T. Brocker, A. Rolink, E. Hirsch, M. Kopf, PI3-Kinase-γ has a distinct and essential role in lung-specific dendritic cell development. *Immunity* **43**, 674–689 (2015). doi:10.1016/j.immuni.2015.09.006 Medline

17. M. Haidinger, M. Poglitsch, R. Geyeregger, S. Kasturi, M. Zeyda, G. J. Zlabinger, B. Pulendran, W. H. Hörl, M. D. Säemann, T. Weichhart, A versatile role of mammalian target of rapamycin in human dendritic cell function and differentiation. *J. Immunol.* **185**, 3919–3931 (2010). doi:10.4049/jimmunol.1000296 Medline

18. H. J. McKenna, K. L. Stocking, R. E. Miller, K. Brasel, T. De Smedt, E. Maraskovsky, C. R. Maliszewski, D. H. Lynch, J. Smith, B. Pulendran, E. R. Roux, M. Teepe, S. D. Lyman, J. J. Peschon, Mice lacking flt3 ligand have deficient hematopoiesis affecting hematopoietic progenitor cells, dendritic cells, and natural killer cells. *Blood* **95**, 3489–3497 (2000). Medline

19. D. Vremec, G. J. Lieschke, A. R. Dunn, L. Robb, D. Metcalf, K. Shortman, The influence of granulocyte/macrophage colony-stimulating factor on dendritic cell levels in mouse lymphoid organs. *Eur. J. Immunol.* **27**, 40–44 (1997). doi:10.1002/eji.1830270107 Medline

20. S. P. Nobs, C. Schneider, M. G. Dietrich, T. Brocker, A. Rolink, E. Hirsch, M. Kopf, PI3-Kinase-γ has a distinct and essential role in lung-specific dendritic cell development. *Immunity* **43**, 674–689 (2015). doi:10.1016/j.immuni.2015.09.006 Medline

21. E. L. Gautier, T. Shay, J. Miller, M. Greter, C. Jakubzick, S. Ivanov, J. Helft, A. Chow, K. G. Elpek, S. Gordonov, A. R. Mazloom, A. Ma'ayan, W.-J. Chua, T. H. Hansen, S. J. Turley, M. Merad, G. J. Randolph, E. L. Gautier, C. Jakubzick, G. J. Randolph, A. J. Best, J. Knell, A. Goldrath, J. Miller, B. Brown, M. Merad, V. Jojic, D. Koller, N. Cohen, P. Brennan, M. Brenner, T. Shay, A. Regev, A. Fletcher, K. Elpek, A. Bellemare-Pelletier, D. Malhotra, S. Turley, R. Jianu, D. Laidlaw, J. Collins, K. Narayan, K. Sylvia, J. Kang, R. Gazit, B. S. Garrison, D. J. Rossi, F. Kim, T. N. Rao, A. Wagers, S. A. Shinton, R. R. Hardy, P. Monach, N. A. Bezman, J. C. Sun, C. C. Kim, L. L. Lanier, T. Heng, T. Kreslavsky, M. Painter, J. Ericson, S. Davis, D. Mathis, C. Benoist;

Immunological Genome Consortium, Gene-expression profiles and transcriptional regulatory pathways that underlie the identity and diversity of mouse tissue macrophages. *Nat. Immunol.* **13**, 1118–1128 (2012). doi:10.1038/ni.2419 Medline

22. A. Schlitzer, N. McGovern, P. Teo, T. Zelante, K. Atarashi, D. Low, A. W. S. Ho, P. See, A. Shin, P. S. Wasan, G. Hoeffel, B. Malleret, A. Heiseke, S. Chew, L. Jardine, H. A. Purvis, C. M. U. Hilkens, J. Tam, M. Poidinger, E. R. Stanley, A. B. Krug, L. Renia, B. Sivasankar, L. G. Ng, M. Collin, P. Ricciardi-Castagnoli, K. Honda, M. Haniffa, F. Ginhoux, IRF4 transcription factor-dependent CD11b+ dendritic cells in human and mouse control mucosal IL-17 cytokine responses. *Immunity* **38**, 970–983 (2013). doi:10.1016/j.immuni.2013.04.011 Medline

23. B. T. Edelson, W. Kc, R. Juang, M. Kohyama, L. A. Benoit, P. A. Klekotka, C. Moon, J. C. Albring, W. Ise, D. G. Michael, D. Bhattacharya, T. S. Stappenbeck, M. J. Holtzman, S.-S. J. Sung, T. L. Murphy, K. Hildner, K. M. Murphy, Peripheral CD103+ dendritic cells form a unified subset developmentally related to CD8alpha+ conventional dendritic cells. *J. Exp. Med.* **207**, 823–836 (2010). doi:10.1084/jem.20091627 Medline

24. D. Eberlé, B. Hegarty, P. Bossard, P. Ferré, F. Foufelle, SREBP transcription factors: Master regulators of lipid homeostasis. *Biochimie* **86**, 839–848 (2004). doi:10.1016/j.biochi.2004.09.018 Medline

25. T. Porstmann, C. R. Santos, B. Griffiths, M. Cully, M. Wu, S. Leevers, J. R. Griffiths, Y.-L. Chung, A. Schulze, SREBP activity is regulated by mTORC1 and contributes to Akt-dependent cell growth. *Cell Metab.* **8**, 224–236 (2008). doi:10.1016/j.cmet.2008.07.007 Medline

26. M. Laplante, D. M. Sabatini, An emerging role of mTOR in lipid biosynthesis. *Curr. Biol.* **19**, R1046–R1052 (2009). doi:10.1016/j.cub.2009.09.058 Medline

27. S. Saglani, S. A. Mathie, L. G. Gregory, M. J. Bell, A. Bush, C. M. Lloyd, Pathophysiological features of asthma develop in parallel in house dust mite-exposed neonatal mice. *Am. J. Respir. Cell Mol. Biol.* **41**, 281–289 (2009). doi:10.1165/rcmb.2008-0396OC Medline

28. M. Plantinga, M. Guilliams, M. Vanheerswynghels, K. Deswarte, F. Branco-Madeira, W. Toussaint, L. Vanhoutte, K. Neyt, N. Killeen, B. Malissen, H. Hammad, B. N. Lambrecht, Conventional and monocyte-derived CD11b(+) dendritic cells initiate and maintain T helper 2 cell-mediated immunity to house dust mite allergen. *Immunity* **38**, 322–335 (2013). doi:10.1016/j.immuni.2012.10.016 Medline

29. J. F. Alcorn, C. R. Crowe, J. K. Kolls, TH17 cells in asthma and COPD. *Annu. Rev. Physiol.* **72**, 495–516 (2010). doi:10.1146/annurev-physiol-021909-135926 Medline

30. J. Douwes, P. Gibson, J. Pekkanen, N. Pearce, Non-eosinophilic asthma: Importance and possible mechanisms. *Thorax* **57**, 643–648 (2002). doi:10.1136/thorax.57.7.643 Medline

31. J. Helft, B. Manicassamy, P. Guermonprez, D. Hashimoto, A. Silvin, J. Agudo, B. D. Brown, M. Schmolke, J. C. Miller, M. Leboeuf, K. M. Murphy, A. García-Sastre, M. Merad, Cross-presenting CD103+ dendritic cells are protected from influenza virus infection. *J. Clin. Invest.* **122**, 4037–4047 (2012). doi:10.1172/JCI60659 Medline

32. J. F. Seymour, J. J. Presneill, Pulmonary alveolar proteinosis: Progress in the first 44 years. *Am. J. Respir. Crit. Care Med.* **166**, 215–235 (2002). doi:10.1164/rccm.2109105 Medline

33. P. L. Shah, D. Hansell, P. R. Lawson, K. B. Reid, C. Morgan, Pulmonary alveolar proteinosis: Clinical aspects and current concepts on pathogenesis. *Thorax* **55**, 67–77 (2000). doi:10.1136/thorax.55.1.67 Medline

34. S. A. Mathie, K. L. Dixon, S. A. Walker, V. Tyrrell, M. Mondhe, V. B. O'Donnell, L. G. Gregory, C. M. Lloyd, Alveolar macrophages are sentinels of murine pulmonary homeostasis following inhaled antigen challenge. *Allergy* **70**, 80–89 (2015). doi:10.1111/all.12536 Medline

35. Y. Gao, S. A. Nish, R. Jiang, L. Hou, P. Licona-Limón, J. S. Weinstein, H. Zhao, R. Medzhitov, Control of T helper 2 responses by transcription factor IRF4-dependent dendritic cells. *Immunity* **39**, 722–732 (2013). doi:10.1016/j.immuni.2013.08.028 Medline

36. E. K. Persson, H. Uronen-Hansson, M. Semmrich, A. Rivollier, K. Hägerbrand, J. Marsal, S. Gudjonsson, U. Håkansson, B. Reizis, K. Kotarsky, W. W. Agace, IRF4 transcription-factor-dependent CD103(+)CD11b(+) dendritic cells drive mucosal T helper 17 cell differentiation. *Immunity* **38**, 958–969 (2013). doi:10.1016/j.immuni.2013.03.009 Medline

37. R. Tussiwand, B. Everts, G. E. Grajales-Reyes, N. M. Kretzer, A. Iwata, J. Bagaitkar, X. Wu, R. Wong, D. A. Anderson, T. L. Murphy, E. J. Pearce, K. M. Murphy, Klf4 expression in conventional dendritic cells is required for T helper 2 cell responses. *Immunity* **42**, 916–928 (2015). doi:10.1016/j.immuni.2015.04.017 Medline

38. M. Greter, J. Helft, A. Chow, D. Hashimoto, A. Mortha, J. Agudo-Cantero, M. Bogunovic, E. L. Gautier, J. Miller, M. Leboeuf, G. Lu, C. Aloman, B. D. Brown, J. W. Pollard, H. Xiong, G. J. Randolph, J. E. Chipuk, P. S. Frenette, M. Merad, GM-CSF controls nonlymphoid tissue dendritic cell homeostasis but is dispensable for the differentiation of inflammatory dendritic cells. *Immunity* **36**, 1031–1046 (2012). doi:10.1016/j.immuni.2012.03.027 Medline

39. E. Amiel, B. Everts, D. Fritz, S. Beauchamp, B. Ge, E. L. Pearce, E. J. Pearce, Mechanistic target of rapamycin inhibition extends cellular lifespan in dendritic cells by preserving mitochondrial function. *J. Immunol.* **193**, 2821–2830 (2014). doi:10.4049/jimmunol.1302498 Medline

40. E. Amiel, B. Everts, T. C. Freitas, I. L. King, J. D. Curtis, E. L. Pearce, E. J. Pearce, Inhibition of mechanistic target of rapamycin promotes dendritic cell activation and enhances therapeutic autologous vaccination in mice. *J. Immunol.* **189**, 2151–2158 (2012). doi:10.4049/jimmunol.1103741 Medline

41. S. M. Houten, R. J. Wanders, A general introduction to the biochemistry of mitochondrial fatty acid β-oxidation. *J. Inherit. Metab. Dis.* **33**, 469–477 (2010). doi:10.1007/s10545-010-9061-2 Medline

42. M. Milovanovic, G. Drozdenko, C. Weise, M. Babina, M. Worm, Interleukin-17A promotes IgE production in human B cells. *J. Invest. Dermatol.* **130**, 2621–2628 (2010). doi:10.1038/jid.2010.175 Medline

43. J. Peng, X. O. Yang, S. H. Chang, J. Yang, C. Dong, IL-23 signaling enhances Th2 polarization and regulates allergic airway inflammation. *Cell Res.* **20**, 62–71 (2010). doi:10.1038/cr.2009.128 Medline

44. M. Murakami, T. Ichisaka, M. Maeda, N. Oshiro, K. Hara, F. Edenhofer, H. Kiyama, K. Yonezawa, S. Yamanaka, mTOR is essential for growth and proliferation in early mouse embryos and embryonic stem cells. *Mol. Cell. Biol.* **24**, 6710–6718 (2004). doi:10.1128/MCB.24.15.6710-6718.2004 Medline

45. M. L. Caton, M. R. Smith-Raska, B. Reizis, Notch-RBP-J signaling controls the homeostasis of CD8- dendritic cells in the spleen. *J. Exp. Med.* **204**, 1653–1664 (2007). doi:10.1084/jem.20062648 Medline

46. B. Kellersch, T. Brocker, Langerhans cell homeostasis in mice is dependent on mTORC1 but not mTORC2 function. *Blood* **121**, 298–307 (2013). doi:10.1182/blood-2012-06-439786 Medline

47. J. Brown, H. Wang, J. Suttles, D. T. Graves, M. Martin, Mammalian target of rapamycin complex 2 (mTORC2) negatively regulates Toll-like receptor 4-mediated inflammatory response via FoxO1. *J. Biol. Chem.* **286**, 44295–44305 (2011). doi:10.1074/jbc.M111.258053 Medline

48. K. Hildner, B. T. Edelson, W. E. Purtha, M. Diamond, H. Matsushita, M. Kohyama, B. Calderon, B. U. Schraml, E. R. Unanue, M. S. Diamond, R. D. Schreiber, T. L. Murphy, K. M. Murphy, Batf3 deficiency reveals a critical role for CD8alpha+ dendritic cells in cytotoxic T cell immunity. *Science* **322**, 1097–1100 (2008). doi:10.1126/science.1164206 Medline

49. M. Pende, S. H. Um, V. Mieulet, M. Sticker, V. L. Goss, J. Mestan, M. Mueller, S. Fumagalli, S. C. Kozma, G. Thomas, $S6K1^{-/-}/S6K2^{-/-}$ mice exhibit perinatal lethality and rapamycin-sensitive 5′-terminal oligopyrimidine mRNA translation and reveal a mitogen-activated protein kinase-dependent S6 kinase pathway. *Mol. Cell. Biol.* **24**, 3112–3124 (2004). doi:10.1128/MCB.24.8.3112-3124.2004 Medline

50. O. Le Bacquer, E. Petroulakis, S. Paglialunga, F. Poulin, D. Richard, K. Cianflone, N. Sonenberg, Elevated sensitivity to diet-induced obesity and insulin resistance in mice lacking 4E-BP1 and 4E-BP2. *J. Clin. Invest.* **117**, 387–396 (2007). doi:10.1172/JCI29528 Medline

51. H. E. Ryan, M. Poloni, W. McNulty, D. Elson, M. Gassmann, J. M. Arbeit, R. S. Johnson, Hypoxia-inducible factor-1alpha is a positive factor in solid tumor growth. *Cancer Res.* **60**, 4010–4015 (2000). Medline

52. S. Kamisuki, Q. Mao, L. Abu-Elheiga, Z. Gu, A. Kugimiya, Y. Kwon, T. Shinohara, Y. Kawazoe, S. Sato, K. Asakura, H.-Y. P. Choo, J. Sakai, S. J. Wakil, M. Uesugi, A small molecule that blocks fat synthesis by inhibiting the activation of SREBP. *Chem. Biol.* **16**, 882–892 (2009). doi:10.1016/j.chembiol.2009.07.007 Medline

53. C. Sinclair, I. Bains, A. J. Yates, B. Seddon, Asymmetric thymocyte death underlies the CD4:CD8 T-cell ratio in the adaptive immune system. *Proc. Natl. Acad. Sci. U.S.A.* **110**, E2905–E2914 (2013). doi:10.1073/pnas.1304859110 Medline

54. K. Breuer, A. K. Foroushani, M. R. Laird, C. Chen, A. Sribnaia, R. Lo, G. L. Winsor, R. E. W. Hancock, F. S. L. Brinkman, D. J. Lynn, InnateDB: Systems biology of innate immunity and beyond—recent updates and continuing curation. *Nucleic Acids Res.* **41**, D1228–D1233 (2013). doi:10.1093/nar/gks1147 Medline

55. D. Szklarczyk, A. Franceschini, S. Wyder, K. Forslund, D. Heller, J. Huerta-Cepas, M. Simonovic, A. Roth, A. Santos, K. P. Tsafou, M. Kuhn, P. Bork, L. J. Jensen, C. von Mering, STRING v10: Protein-protein interaction networks, integrated over the tree of life. *Nucleic Acids Res.* **43** (D1), D447–D452 (2015). doi:10.1093/nar/gku1003 Medline

56. S. Li, Y. Park, S. Duraisingham, F. H. Strobel, N. Khan, Q. A. Soltow, D. P. Jones, B. Pulendran, Predicting network activity from high throughput metabolomics. *PLOS Comput. Biol.* **9**, e1003123 (2013). doi:10.1371/journal.pcbi.1003123 Medline

57. E. Fahy, S. Subramaniam, H. A. Brown, C. K. Glass, A. H. Merrill Jr., R. C. Murphy, C. R. H. Raetz, D. W. Russell, Y. Seyama, W. Shaw, T. Shimizu, F. Spener, G. van Meer, M. S. VanNieuwenhze, S. H. White, J. L. Witztum, E. A. Dennis, A comprehensive classification system for lipids. *J. Lipid Res.* **46**, 839–862 (2005). doi:10.1194/jlr.E400004-JLR200 Medline

58. K. Liu, G. D. Victora, T. A. Schwickert, P. Guermonprez, M. M. Meredith, K. Yao, F. F. Chu, G. J. Randolph, A. Y. Rudensky, M. Nussenzweig, In vivo analysis of dendritic cell development and homeostasis. *Science* **324**, 392–397 (2009). Medline